

# Integrating brain and biomechanical models - a new paradigm for understanding neuro-muscular control

**Sebastian James**<sup>1,2</sup>, **Chris Papapavlou**<sup>5</sup>, **Alexander Blenkinsop**<sup>1,2</sup>,  
**Alexander Cope**<sup>3</sup>,

**Sean Anderson**<sup>2,4</sup>, **Konstantinos Moustakas**<sup>5</sup>, **Kevin Gurney**<sup>1,2,\*</sup>

<sup>1</sup> *Adaptive Behaviour Research Group, Department of Psychology, The University of Sheffield, Sheffield, UK*

<sup>2</sup> *Insigneo Institute for in-silico Medicine, The University of Sheffield, Sheffield, UK*

<sup>3</sup> *Department of Computer Science, The University of Sheffield, Sheffield, UK*

<sup>4</sup> *Department of Automatic Control Systems Engineering, The University of Sheffield, Sheffield, UK*

<sup>5</sup> *Department of Electrical and Computer Engineering, The University of Patras, Patras, Greece*

Correspondence\*:

Kevin Gurney

Department of Psychology, The University of Sheffield, Western Bank, Sheffield, S10 2TP, UK, k.gurney@sheffield.ac.uk

## 2 ABSTRACT

To date, realistic models of how the central nervous system governs behaviour have been restricted in scope to the brain, brainstem or spinal column, as if these existed as disembodied organs. Further, the model is often exercised in relation to an *in vivo* physiological experiment with input comprising an impulse, a periodic signal or constant activation, and output as a pattern of neural activity in one or more neural populations. Any link to behaviour is inferred only indirectly via these activity patterns. We argue that to discover the principles of operation of neural systems, it is necessary to express their behaviour in terms of physical movements of a realistic motor system, and to supply inputs that mimic sensory experience. To do this with confidence, we must connect our brain models to neuro-muscular models and provide relevant visual and proprioceptive feedback signals, thereby closing the loop of the simulation. This paper describes an effort to develop just such an integrated brain and biomechanical system using a number of pre-existing models. It describes a model of the saccadic oculomotor system incorporating a neuromuscular model of the eye and its six extraocular muscles. The position of the eye determines how illumination of a retinotopic input population projects information about the location of a saccade target into the system. A pre-existing saccadic burst generator model was incorporated into the system, which generated motoneuron activity patterns suitable for driving the biomechanical eye. The model was demonstrated to make accurate saccades to a target luminance under a set of environmental constraints. Challenges encountered in the development of this model showed the importance of this integrated modelling approach. Thus, we exposed shortcomings in individual model components which were only apparent when these

were supplied with the more plausible inputs available in a closed loop design. Consequently we were able to suggest missing functionality which the system would require to reproduce more realistic behaviour. The construction of such closed-loop animal models constitutes a new paradigm of *computational neurobehaviour* and promises a more thoroughgoing approach to our understanding of the brain's function as a controller for movement and behaviour.

Keywords: integrated brain biomechanics neuromuscular oculomotor saccade basal ganglia

## 1 INTRODUCTION

Note: Changes based on Reviewer 1's comments are in this colour. For Reviewer 2 we use this colour.

The field of computational neuroscience has provided many *systems models* of the brain (Arai et al., 1994; Gancarz and Grossberg, 1998; Hazy et al., 2007; Blenkinsop et al., 2017). We refer to these as *mechanistic computational models*, meaning models which consist of populations of neural elements, interconnected in a biologically plausible manner, which simulate the operation of the brain. Whilst they differ in scale and complexity, these models all seek to describe the fundamental mechanisms behind common animal behaviours such as locomotion, threat evasion, reaching or feeding. However, none of the models cited here actually reproduce these behaviours. In each case, the activity in a certain population of neurons is taken to be representative of a behavioural outcome. In some cases, it is reasonable to take the activity of an internal population within the brain model as being representative of the induced behaviour. For example, a choice made in a *go/no-go* task could be determined from activity in a population within a basal ganglia model (Nambu et al., 1990; Kühn et al., 2004). The decision to *go* is selected by a reduction of activity in this population; maintenance of activity implies *no-go*. To validate the model, the error rates which it generates could be compared with experimentally determined error rates in primate subjects. We refer to this as an *output assumption model* because the output is assumed to signify behaviour. (An *input assumption model* assumes that sensory input produces some particular form of neural activity in an input population of the model.)

However, we may be interested in reproducing accurate simulated *trajectories*, in order to find out how degradation of parts of the model affect movement. In Parkinson's Disease, degradation of the dopamine neurons originating in the substantia nigra pars compacta (SNc) causes diskinesia (Galvan and Wichmann, 2008), as well as abnormal network activity in the basal ganglia (Brown et al., 2001; McCarthy et al., 2011). Sufferers of the disease would be expected to produce abnormal decision-making and movement trajectories in a reach-to-the-correct-target task such as the one described in James et al. (2017). A model which sought to explore in detail the effects of the SNc degradation both on the decision making and on the movement dynamics would need a physically accurate virtual arm, as well as physically realistic sensory input for the brain. This is no less than a complete model of those sections of the brain and body which act to fulfil the task. Such a modelling effort, if successful, would result in a virtual robot capable of expressing behaviour *in response to sensory input from its environment*. This would represent a paradigm shift in the field of computational neuroscience worthy of the new name of *computational neurobehaviour*.

In an attempt to build a model combining brain, realistic biomechanics and sensory feedback, we sought to extend our previous work modelling the oculomotor system by adding a virtual, biomechanical eye model able to make physically realistic movements. The rotational state of the eye would then determine how visual features in the virtual world were projected back into the brain model. The existing model (Cope et al., 2017) is already able to capture sensory input and convert it into a neural signal, assumed to specify the target of a *saccadic eye movement*; a fast movement of the eyes which directs the fovea to

64 a region of interest in the field of view. The oculomotor system is an excellent candidate for modelling  
65 because its movements can be specified with only three degrees of freedom, making it one of the simplest  
66 neuro-muscular systems in the body. It is nevertheless behaviourally interesting, as saccadic eye movements  
67 reveal information about decision making at a subconscious level (Deubel and Schneider, 1996; Reppert  
68 et al., 2015; Marcos and Genovesio, 2016). The modelling of the oculomotor system is served by a large  
69 body of behavioural data describing saccades (Tipper et al., 2001; Walker et al., 1997; Casteau and Vitu,  
70 2012), many anatomical studies of the neural substrates involved (Meredith and Ramoa, 1998; Isa, 2002;  
71 Isa and Hall, 2009) and electrophysiological data linking these together (Hepp and Henn, 1983; Dorris et al.,  
72 1997; McPeek et al., 2003; Vokoun et al., 2011). Furthermore, in the context of building *behaving* systems,  
73 a necessary part of any model for which the behaviour requires visual attention and decision making is a  
74 realistic mechanism for gathering visual information. This is obvious from extrinsic considerations—a  
75 subject must look at a scene to make decisions or navigate within it. It also follows for *intrinsic* reasons.  
76 For example, Howard and Tipper (1997) showed that visual cues affect reach trajectories and the same  
77 group later demonstrated that reaching affects the saccadic system (Tipper et al., 2001) suggesting a close  
78 relationship between these neural systems. **Building a behaving oculomotor system will therefore assist**  
79 **future computational neurobehavioural modelling efforts that involve reaching.**

80 Many neural populations are involved in the coding of saccadic eye movements, only a very brief  
81 overview is given here; for a review, see Munoz (2002). One pathway takes information from the retina  
82 directly into the superficial layers of the superior colliculus in the brainstem (Sterling, 1971; Linden and  
83 Perry, 1983; Wu et al., 1994). Activity within the superior colliculus then excites neurons in the pons,  
84 medulla and rostral mid-brain (Sparks, 2002). and **finally the motor neurons** which innervate the extraocular  
85 muscles (Fuchs and Luschei, 1970; Sparks, 2002). This direct pathway is responsible for the low latency  
86 saccades called express saccades (Schiller et al., 1987; Edelman and Keller, 1996). Information from the  
87 retina is also processed by visual cortex which feeds through to the frontal eye fields in which activity is  
88 related to reflexive and voluntary saccades (Schall and Thompson, 1999). Activity build-up in the frontal  
89 eye fields is transferred to the intermediate layers of the superior colliculus (Stanton et al., 1988b) and is  
90 also processed by the basal ganglia, which participates in the selection of the winning saccade end point  
91 (Stanton et al., 1988a; Hikosaka et al., 2000). Although both cortical and subcortical paths produce a  
92 saccade target signal in the superior colliculus, it is also possible for animals to make relatively normal  
93 saccades even after the colliculus has been ablated (Wurtz and Goldberg, 1972; Aizawa and Wurtz, 1998),  
94 though express saccades are lost with collicular lesions (Schiller et al., 1987). This makes the superior  
95 colliculus a perplexing structure, being both critically involved in saccade target specification (Sparks and  
96 Nelson, 1987) and saccade dynamic control (Waitzman et al., 1991; Goossens and van Opstal, 2012) and  
97 yet dispensable. The ‘backup pathway’ likely incorporates the oculomotor vermis and fastigial oculomotor  
98 region of the cerebellum which are known to participate in the specification, dynamics and adaptation of  
99 saccadic eye movements (Kleine, 2003; Takagi et al., 1998).

100 There is a long history of modelling the oculomotor system. For a comprehensive review, see Girard and  
101 Berthoz (2005). Models of individual **sub-systems** have been proposed for brainstem (Robinson, 1975;  
102 Scudder, 1988; Gancarz and Grossberg, 1998), cerebellum (Quaia et al., 1999; Dean, 1995; Dean et al.,  
103 1994) and superior colliculus (Massone, 1994; Arai et al., 1994; Morén et al., 2013; Marino et al., 2012).  
104 More recently, combined models have also been developed incorporating sensory input (Cope et al., 2017)  
105 and driving **a second order differential equation** representing the eye (Tabareau et al., 2007; N’Guyen  
106 et al., 2014; Thurat et al., 2015). None of these models has yet fully closed the loop to produce a behaving  
107 system operating freely within its environment. We argue that developing integrated, closed-loop models of

108 behaving systems offers insights into the operation of neural systems that are not available from input- or  
109 output-assumption models.

## 2 MATERIAL & METHODS

110 The integrated brain and biomechanical model described here is a development of the model in Cope  
111 et al. (2017), referred to here as the Cope-Chambers model. This was a rate-coded neural network model  
112 incorporating retinal populations, frontal eye fields (FEF), the basal ganglia (BG), and the superior colliculus  
113 (SC). The Cope-Chambers model takes as *input* the positions of luminances (of fixed shape and intensity)  
114 on a topographic map. Whilst certain assumptions were made about the input—that a luminant input excites  
115 activity on a retinotopic layer, with computer code carrying out the transformation achieved in the brain by  
116 a neural connectivity map (Thivierge and Marcus, 2007)—it is nonetheless *not* an input-assumption model  
117 according to our definition because the activity generated in the neural input layer is modelled as a response  
118 to the luminances, rather than being crafted. In the Cope-Chambers model, the centroid of the activity in  
119 the deep layers of superior colliculus was assumed to accurately encode the location of the eye at the end  
120 of the saccade (Wurtz and Goldberg, 1972; Robinson, 1972; Van Gisbergen et al., 1987; McIlwain, 1982).  
121 This location was used to recalculate the positions of the luminances in the eye's frame of reference at each  
122 time step. Because a pattern of neural activity in the output population was assumed to have a behavioural  
123 outcome, it was thus an *output-assumption model*. The model included no brainstem populations other  
124 than superior colliculus, nor a neuromuscular model.

125 To the Cope-Chambers model, we added a brainstem model and a biomechanical eye model. The rate-  
126 coded brainstem model was taken from the literature (Gancarz and Grossberg, 1998) as the best-of-breed  
127 saccadic burst generator (Girard and Berthoz, 2005). The biomechanical eye was implemented using the  
128 biomechanical modelling framework OpenSim; the brain and brainstem were modelled using the SpineML  
129 toolchain. These will be described below, along with a review of the Cope-Chambers model, but first we  
130 will give a description of the co-ordinate systems.

### 131 2.1 Co-ordinates in the world

132 Before describing the biomechanical eye and the brain model, which consisted of retinotopically mapped  
133 neural sheets, we describe the co-ordinate system used in the world. The eye was located at the origin of a  
134 three-dimensional, right-handed Cartesian co-ordinate system, with its fovea directed in the  $-z$  direction.  
135 There was a notional spherical screen which was also centred at the origin of the co-ordinate system and  
136 had a radius of 50 (in arbitrary units). The *fixation point* was the point on the screen at which the eye  
137 was initially directed. Onto the screen were projected target luminances, each of which having a position  
138 described by two co-ordinates;  $\theta_x^t$ , a rotation of the horizon plane about the  $x$  axis, and  $\theta_y^t$ , a rotation of the  
139 meridian plane about the  $y$  axis. The position is the intersection of these rotated planes with the spherical  
140 screen (disregarding the intersection point of these three surfaces behind the eye). Note that a luminance  
141 with positive  $\theta_x^t$  was above the horizon of this world; one whose  $\theta_y^t$  was positive lay to the left of the  
142 world's meridian. For this reason, many of the figures in this paper are plotted with  $-\theta_y$  on the  $x$ -axis and  
143  $\theta_x$  on the  $y$ -axis so that targets that lay up and to the right in the world do so in the graphs, also.

144 Luminances were crosses of height and width subtending  $\pm 3^\circ$  and whose 'bars' were  $2^\circ$  thick. Lumi-  
145 nances were oriented like + symbols with their vertical bar aligned with the meridian plane and their  
146 horizontal bar aligned with the horizon.

147 The eye's frame of reference was initially aligned with the world's frame of reference. At each timestep,  
148 the eye's rotational state (described by the Euler rotations  $\theta_x$ ,  $\theta_y$ ,  $\theta_z$ ) was used to translate the three  
149 dimensional Cartesian co-ordinates of the luminances in the world frame into co-ordinates in the eye frame.  
150 The luminance co-ordinates in the eye's frame of reference were used to determine the input to the brain  
151 model.

## 152 2.2 Existing brain model

153 The brain model, excluding the brainstem, is a re-implementation of the Cope-Chambers model, of  
154 reflexive saccadic behaviour (Cope et al., 2017). Reflexive saccades are fast eye movements elicited by  
155 abrupt changes in the peripheral visual scene (reflexive saccades can occur also as a result of auditory  
156 and somatosensory stimuli, but these modalities are ignored in this model). A reflexive saccade has a  
157 starting position defined by the initial orientation of the eye and an end-point position in which the eye  
158 is directed towards a new target. Regardless of the number of targets within the visual scene, the brain  
159 must choose one location as the end-point, because the eyes can look only in one direction at a time. The  
160 functionality reproduced by the Cope-Chambers model is 'the selection of the best target end-point for  
161 a reflexive saccade'. A competition such as this between incompatible movements is often referred to  
162 as an *action selection* problem (Norman and Shallice, 1986; Maes, 1989; Redgrave et al., 1999). The  
163 Cope-Chambers model is therefore a model of action-selection in the oculomotor system for reflexive  
164 saccades. One hypothesis for the rôle played by the basal ganglia (BG) is that the system performs *action*  
165 *selection* (Mink, 1996; Redgrave et al., 1999; Hikosaka et al., 2000). The Cope-Chambers model places the  
166 BG at the centre of the oculomotor system; this follows the known anatomy of the region (Hikosaka et al.,  
167 2000) and provides a mechanism for action selection of the best saccade. The BG receives input indirectly  
168 from the superior colliculus, which has a retinotopic arrangement (Ottos et al., 1986).

169 The BG receives excitatory inputs directly from retinotopic regions of the cortex including the frontal eye  
170 fields (FEF), supplementary eye fields (SEF), lateral intraparietal cortex (LIP) and dorsolateral prefrontal  
171 cortex. The dorsolateral prefrontal cortex, which participates in voluntary saccades (Funahashi et al., 1993;  
172 Munoz and Everling, 2004), is not modelled because the model concerns reflexive rather than voluntary  
173 eye movements. Several other regions of the brain that are associated with eye movements are also omitted  
174 from the model. The early visual processing stream in cortex, from V1, through to the LIP is subsumed into  
175 a 'sustained retinal' signal which arrives at FEF. The justification here is that the model reacts to simple  
176 luminant targets and does not need to carry out the feature extraction performed by these visual areas. The  
177 supplementary eye fields are involved in the programming of saccade sequences (Tehovnik et al., 2000)  
178 and memory guided saccades (Chen and Wise, 1995; Schlag, 2002). Lesions of SEF do not affect visually  
179 guided saccades (Gaymard et al., 1998) and so the SEF is also omitted from the model.

180 Fig. 1(a) shows the macroscopic architecture of the Cope-Chambers model. The figure shows the  
181 relationships between the retinal input populations, the FEF, the populations comprising the BG sub-system  
182 (the red border indicates that the box represents a number of populations as a sub-system), the thalamus and  
183 the superior colliculus. Excitatory connections are indicated with arrow heads; inhibitory connections with  
184 circles in place of the arrow heads. The blue and green connection lines indicate two thalamo-basal ganglia  
185 loops, one cortical loop through FEF (green), the other a sub-cortical loop through SC. It is important to  
186 note that although they are given different colours in the diagram, these loops are in no way independent,  
187 with loop activity combining both in thalamus and in the basal ganglia and a direct excitatory, feed-forward  
188 connection from FEF to SC.

189 The basal ganglia sub-system is the most complex component of the Cope-Chambers model. The BG  
190 model is based on previous work (Gurney et al., 2001b,a) and is referred to as the GPR model. The GPR model  
191 incorporates the following main components of the primate BG (Mink, 1996; Wickens, 1997): (i)  
192 The striatum (the main input station to the BG) which is divided into two iterdigitated populations of  
193 projection neurons expressing primarily D1 or D2-type dopaminergic receptors (named Str\_D1 and Str\_D2);  
194 (ii) The subthalamic nucleus (STN); (iii) the external segment of the globus pallidus (GPe); (iv) the output  
195 nucleus relevant for saccadic control—the substantia nigra pars reticulata (SNr) (Hikosaka et al., 2000).

196 The connectivity of the GPR model [Fig. 1(b)] is constrained by the known anatomy and physiology of  
197 the BG (Bolam et al., 2000). Physiologically, the only source of glutamate within the BG is the STN, whose  
198 projections are therefore excitatory; all other nuclei have GABAergic projection neurons and are therefore  
199 inhibitory. The cortex sends glutamatergic projections to both the Str\_D1 striatal population, which projects  
200 preferentially to the SNr, and to Str\_D2, which projects primarily to GPe (Gerfen et al., 1990). The cortex  
201 also projects to the STN, which sends diffuse projections to the SNr and GPe (Parent and Hazrati, 1993).  
202 The GPe projects to the SNr and also projects back to the STN, completing a GPe-STN loop.

203 The GPR model is arranged into ‘action channels’; Fig. 1(b) shows an example network containing three  
204 channels. It is between these channels that competition occurs, with the winning channel succeeding in  
205 reducing activity in the output nucleus, SNr, and thereby disinhibiting its target. The complete connectivity  
206 pattern for this small network is shown in Fig. 1(b); the left channel in cortex innervates the left channels  
207 of Str\_D1, STN and Str\_D2. Connections are one-to-one, so it follows that the middle channel of cortex  
208 innervates the middle channels of STN and the striatal populations and the right channel of cortex innervates  
209 right channels in striatum and STN. Striatal population channels also inhibit SNr and GPe on a one-to-one  
210 basis and GPe feeds inhibition to SNr and STN in a one-to-one manner. The outputs from STN however  
211 are not one-to-one. The output from all channels of STN is summed together and then the sum is fed into  
212 each channel of SNr and GPe. This models the diffuse excitation from STN which has been observed in  
213 the BG (Parent and Hazrati, 1993).

214 Within the BG, there are several mechanisms supporting competitive processing for selecting channels  
215 whose inhibitory output should be reduced. The selection mechanism of the GPR model is the ‘off-centre,  
216 on-surround’ scheme proposed by Mink and Thach (1993). The ‘on-surround’ is provided by diffuse,  
217 excitatory projections from the STN to the SNr. Focussed inhibition from the Str\_D1 neurons in striatum  
218 contributes the ‘off-centre’ part of the mechanism. This arrangement leads to selection behaviour via a  
219 release of target inhibition, since channels that have strong salience (input) have weak output at the level of  
220 SNr, and channels with weak salience have enhanced output.

221 The GPe is not included in the centre-surround circuit described above, but still plays a key rôle in  
222 selection. Operating alone, the Str\_D1/STN/SNr circuit can suffer from the following problem: if the input  
223 for all channels is relatively high, then the diffuse projection from STN, which effectively supplies a sum  
224 of *all* of the STN inputs to each channel in SNr, will provide so much excitation that Str\_D1 may become  
225 unable to inhibit one of the channels in SNr and selection may become impossible. Gurney et al. (2001b,a)  
226 showed that the inhibitory feedback from GPe to STN acts as an ‘automatic gain control’ to help prevent  
227 this from occurring.

228 At the neuronal level, the STN, GPe and SNr have tonic output levels (Chevalier and Deniau, 1990;  
229 DeLong et al., 1985; Kita and Kitai, 1991). This is modelled using piecewise linear output functions  
230 with zero offsets,  $c$  (see Eq. 6) but with noise added to the input. In striatum, Str\_D1 and Str\_D2 have  
231 positive offset  $c$ , mimicking the so-called ‘down-state’ of medium spiny neurons which have a resting

232 potential far below spiking threshold and require co-ordinated input to generate action potentials (Wilson  
 233 and Kawaguchi, 1996). In addition, the Str\_D1 and Str\_D2 neurons are influenced by dopamine in different  
 234 ways; facilitating cortico-striatal transmission at medium spiny neurons with D1 receptors (Hernndez-Lpez  
 235 et al., 1997; Gonon, 1997) and reducing transmission at those with D2 receptors (Delgado et al., 1999).  
 236 These effects are modelled using a dopamine parameter,  $d$ , which modulates the input activations  $a_{in}^{D1}$  and  
 237  $a_{in}^{D2}$  as:

$$a_{in}^{D1} = (0.2 + d)A \quad (1)$$

$$a_{in}^{D2} = (1 - d)A \quad (2)$$

238 where  $A$  is the input activation (see also Eqns. 10 & 11). For the ‘normal, healthy’ value for  $d$  of 0.7,  
 239 Str\_D1 activation is relatively enhanced ( $0.9A$ ); Str\_D2 activation is one third of this value ( $0.3A$ ). The  
 240 major effect of this difference in the relative strength of the activity in Str\_D1 versus Str\_D2 is simply that  
 241 a change in the level of activity in Str\_D1 affects the off-centre, on-surround mechanism. The effect of  
 242 varying the input into Str\_D2 is much more subtle, with only a small change in the amount of inhibition fed  
 243 from GPe into STN (via a focussed, one to one connection) being affected by the change, along with a  
 244 small change in the inhibition fed into SNr from GPe (also via a one to one connection). It is not possible  
 245 to clearly describe the dynamic effect of the dopamine parameter as being due to any single population,  
 246 because the activity is recurrently connected through multiple loops. Thus, a line of reasoning such as  
 247 “reduced activity for a luminance in Str\_D2 will lead to less inhibition in that region in GPe, which means  
 248 that there will be higher activity there, and hence more inhibition for that region passed to STN leading us  
 249 to expect less activity in STN” is verified by running a suitable simulation with the model, but the effect is  
 250 small. Note that the effect of dopamine in the model is only to modulate the strength of cortico-striatal  
 251 synapses; no learning is modelled and so the significance of dopamine as a prediction error signal is outside  
 252 the scope of the current work.

254 The GPR model in Fig. 1(b) has only three channels, with the focussed inhibition from striatum to SNr  
 255 and GPe defined by a simple one-to-one scheme. The action channels represent discrete, incompatible  
 256 motor action choices. In the oculomotor model, an action channel represents the end-point of saccade,  
 257 and the competition carried out in the basal ganglia is between potential saccade end-points. However,  
 258 eye movements have a *continuous* end-point space; the eye can rotate to any orientation within its  
 259 biomechanically permissible range. Some end-points within this range are mutually exclusive—it’s not  
 260 possible to look to the left and to the right simultaneously—but *nearby* end-points are not necessarily  
 261 incompatible. A small enough error in the end-point of a saccade will not prevent the eye from foveating on  
 262 a target as the foveal region of high visual acuity is not infinitesimally small. To cope with this requirement,  
 263 the populations within the oculomotor basal ganglia are conceived of as two-dimensional topographic  
 264 grids of leaky integrator neural elements. Activity in each element corresponds to a spatial location in the  
 265 visual field. Neighbouring elements correspond to locations which are close to each other in the visual field.  
 266 Focussed one-to-one projections in the GPR model are replaced by projective fields with many weighted  
 267 connections. Specifically, each unit in Str\_D1 projected to a counterpart SNr<sub>j</sub> in SNr with some weight  
 268  $w_{max}$ , but also connected to neighbouring nodes in SNr with a weight given by  $w_{max} \cdot G(d)$ , where  $G(d)$  is  
 269 a circularly symmetric, 2D-Gaussian which is a function of distance  $d$  from SNr<sub>j</sub> [Fig. 1(c)]. A similar  
 270 scheme applied for the connectivity from Str\_D2 to GPe and for a number of the other connections in the  
 271 Cope-Chambers model; in the SpineML implementation of the model, this connectivity scheme is named  
 272 ‘GaussianKernel’. Fig. 2 shows a schematic of the SpineML implementation of the model, based on a  
 273 diagram output directly from SpineCreator. Populations for Str\_D1, Str\_D2, STN, SNr and GPe are shown  
 274 within the ‘Basal Ganglia’ box. Input comes into the model via the ‘World’ population and the output

275 population is SC\_deep. Compare this diagram with Figs. 1(a) & (b). Fig. 2 expands the ‘SC’, ‘BG’ and  
276 ‘slow retinal’ boxes from Fig. 1(a).

277 The frontal eye fields (FEF) are a key cortical area for the generation of saccadic eye movements (Hikosaka  
278 et al., 2000; Tehovnik et al., 2000; Robinson and Fuchs, 1969; Bruce and Goldberg, 1985). Saccadic targets  
279 are mapped retinotopically over its surface (Robinson and Fuchs, 1969; Bruce and Goldberg, 1985; Sabes  
280 et al., 2002), and increased neural activity at a location in the map precedes a saccade to that location.  
281 Importantly, the FEF is also associated with visual decision making (Thompson and Bichot, 2005; Schall  
282 et al., 1995; Monosov et al., 2008; Cohen et al., 2009). Thus, in a saccade choice, increased FEF activity is  
283 predictive of the eye movement whether correct or incorrect (Thompson et al., 2005), rather than of the  
284 correct response.

285 FEF neurons can be divided in to three functional groups, related to whether their activity corresponds  
286 with visual stimuli, motor action, or both (Segraves and Goldberg, 1987). The Cope-Chambers model  
287 simplifies this categorisation using a single layer of 50 by 50 units representing the mean of all three  
288 groups. This layer therefore responds to both visual stimuli and the buildup of activity associated with  
289 motor (saccadic) action. The retina provides a persistent luminance signal into the FEF through the dorsal  
290 visual pathway (Ungerleider and Mishkin, 1982) which is abbreviated in this model to a direct connection  
291 with delay.

292 The FEF provides input into the BG (Saint-Cyr et al., 1990) (to Str\_D1, Str\_D2 and STN) which, in turn,  
293 projects back to thalamus in a retinotopically organised way (Middleton and Strick, 2000; Lynch et al.,  
294 1994). In addition, the thalamic targets of this path are regions with strong reciprocal connections to the  
295 FEF (McFarland and Haber, 2002). In this way, the FEF forms channel-based loops through basal ganglia  
296 of the kind described above. Such circuits formed the basis of the model of Humphries and Gurney (2002).  
297 The thalamo-cortical loop may be thought of as an integrator of information, whose gain is modulated by  
298 inhibition from basal ganglia (Chambers et al., 2012; Cope and Gurney, 2011).

299 The superior colliculus (SC) is a sub-cortical nucleus which also plays a critical rôle in the generation  
300 of saccades (Hikosaka and Wurtz, 1983). Both FEF and SC have direct connections to the saccadic burst  
301 generator (SBG, see Sect. 2.3). If either is lesioned, the other can direct gaze, following a period of  
302 adjustment (Latto, 1977), albeit with some persistent deficits. The SC is also a direct target of output  
303 from the SNr (Jayaraman et al., 1977; Jiang et al., 2003) and can be influenced by the action selection  
304 mechanisms of the BG. In particular, it forms a loop with BG, but unlike its cortical counterpart in FEF, the  
305 input to basal ganglia comes via the thalamus [Fig 1(a), blue arrows].

306 While the SC has seven alternating cell- and fibre-rich layers (Wurtz and Albano, 1980), in most  
307 cases these are divided into the ‘superficial’ and ‘deep’ layers, which have significantly different response  
308 properties. Cells in the superficial layers, which receive input from the retina, are mainly visually responsive,  
309 with a preferred response to phasic events (luminance onsets and offsets) and movement on the visual  
310 field (Goldberg and Wurtz, 1972). In contrast, cells in the deep layers receive multi-modal input, including  
311 inhibitory input from the output structures of the BG (Jayaraman et al., 1977), and are directly involved  
312 in the generation of saccadic eye movements. Saccade related activity in the deep layers appears to  
313 generate saccades through ‘population coding’, with a weighted sum of activity across the retinotopy of SC  
314 determining the saccade target (Lee et al., 1988; van Opstal and van Gisbergen, 1990; Mays and Sparks,  
315 1980). The deep layers of SC receive input from the FEF in a topographic manner (Stanton et al., 1988a;  
316 Sommer and Wurtz, 2000).

317 The SC in the Cope-Chambers model is based on the the model described in Arai and Keller (2005), with  
318 the difference that the SNr input to the SC is generated by the BG model, rather than being hand-crafted.  
319 The SC model has a superficial and a deep layer, each of which is a 2-D array of 50 by 50 leaky integrator  
320 units arranged in the same retinotopic manner as the FEF (Wurtz and Albano, 1980).

321 The Cope-Chambers model incorporates a special connectivity pattern for visual input via cortical (FEF)  
322 and sub-cortical (thalamus) pathways. Due to the retinotopic mapping (Sect. 2.2.2), foveal luminances  
323 deliver a strong signal to the BG; roughly one third of the map is activated for the foveal targets used in  
324 this work (Fig. 3, red cross). This makes it virtually impossible for a peripheral target (Fig. 3, yellow cross)  
325 to win selection in the BG. Even if the peripheral target competed successfully to generate a saccade, this  
326 process would cause a significant delay, leading to latencies much larger than those observed experimentally.  
327 To overcome this problem, the Cope-Chambers model incorporates a mechanism in which the synaptic  
328 strength of connections between FEF, thalamus and striatum are reduced close to the fovea according to a  
329 shifted hyperbolic tangent. This connection is named ‘DecayingAtFovea’ in the SpineML implementation  
330 and follows a modified sigmoidal curve rather than tanh. In either case, the relation is ‘S-shaped’ and  
331 normalised to the range [0 1]. Far from the fovea (where the S-shaped curve has the value  $\approx 1$ ), the  
332 connectivity pattern looks almost identical to a one-to-one connection.

333 Input to the Cope-Chambers model is provided through a simple retina model which directly samples  
334 from a larger ‘world array’ of pixel values. In the current model, the input for the retina is named ‘World’  
335 and is the retinotopic projection [Fig. 2(b)] of the eye’s field of view of the world [Fig. 2(a)] and the  
336 luminant targets therein. The raw input in ‘World’ is fed into a population which adds noise, and then  
337 via a delayed connection to FEF (the sustained retinal input path), to simulate processing through the  
338 dorsal visual stream. It is also fed, without substantial delay, into two leaky integrator layers (Retina\_1  
339 and Retina\_2) with different time constants, with the more slowly reacting layer (Retina\_2) inhibiting its  
340 faster counterpart. The faster layer responds quickly to the appearance of a prolonged stimulus before it  
341 is inhibited by the slow layer, forming a phasic response to stimulus onset. The mechanism ensures that  
342 phasic rather than tonic responses arrive at the superficial SC from the retina.

343 The output of the Cope-Chambers model is determined by the activity in the SC\_deep population. The  
344 activity in SC\_deep is first transformed from retinotopic co-ordinates into the Cartesian co-ordinates. The  
345 centroid of the activity is then computed. The position of this centroid in the Cartesian frame determines  
346 the saccadic end-point. The current model differs in that it does not compute a centroid, instead feeding the  
347 SC\_deep activity into the saccadic burst generator.

348 The Cope-Chambers model was parameterised by tuning the model to perform a prosaccade task in which  
349 a fixed luminance point is fixated by teh model. After a fixed duration, the fixation point was extinguished  
350 and a target point of fixed luminance was presented. The model was tuned so that the latency between the  
351 presentation of the target and the initiation of an eye movement matched experimental data (Reulen, 1984),  
352 while also matching the electrophysiological evidence of activity in a variety of brain regions. The tuning  
353 of the BG model attempted to preserve as closely as possible the weights used in the original paper. Further  
354 details on the parameterisation of the Cope-Chambers model are in Cope et al. (2017).

### 355 2.2.1 Components

356 With the exceptions of the World and FEF\_add\_noise populations, each neural element represents an  
357 activation; the activation is governed by a first order differential equation specified in a *SpineML component*.  
358 SpineML, which will be outlined in Sect. 2.5, provides a means to mathematically define the five distinct  
359 components in use in the brain model.

360 The *LINlinear* component governs the activation  $a$  with a first order leaky integrator differential equation:

$$\dot{a} = \frac{1}{\tau}(a_{in} - a) \quad (3)$$

361 where  $\tau$  is the time constant for the neural activation and  $a_{in}$  is the input to the neural element.  $a_{in}$  is  
362 defined by an activation input and a shunting inhibition input according to:

$$a_{in} = A(1 - s_a) + \alpha R_N \quad (4)$$

363 Here,  $A$  is the activation input and  $s_a$  is the shunting inhibition state variable whose value is related to the  
364 shunting input,  $S$  by

$$s_a = \begin{cases} S & S \leq 1 \\ 1 & S > 1 \end{cases} \quad (5)$$

365  $R_N$  is a random number drawn from a standard normal distribution ( $\sigma=1$ ,  $\mu=0$ ) and introduces noise to the  
366 activation of the neural element, with the parameter  $\alpha$  controlling the noise amplitude.

367 The output,  $y$ , of LINlinear is related to the activation  $a$  by the piecewise linear transfer function

$$y(a) = \begin{cases} 0 & a < c \\ a - c & c \leq a \leq 1 + c \\ 1 & a > 1 + c \end{cases} \quad (6)$$

368 where  $c$  is a parameter defining the offset of the transfer function. If  $c < 0$ , then for zero activation ( $a = 0$ ),  
369 the output will be positive. This simulates the effect of a neural population having tonic firing. If  $c > 0$   
370 then the output will be zero until the activation exceeds  $c$ , simulating neurons which only fire when driven  
371 by excitatory input.

372 The *LINret* component used for the retinal populations is similar to the LINlinear component, but with no  
373 intrinsic noise and no shunting inhibitory input. It has a neural input which is identical to the activation  
374 input  $A$ :

$$a_{in} = A \quad (7)$$

375 The *LINexp* component is a leaky integrator with an exponential transfer function. It shares the same  
376 differential equation with LINlinear, but has a different input equation and a different output transfer  
377 function. It has the following equation for the neural element input  $a_{in}$ :

$$a_{in} = [A + N(a - V_r^-)](1 - S) + 0.01R_N \quad (8)$$

378 where  $A$  is the activation input and  $N$  is an input which is modulated by  $V_r^-$ , a reversal potential, and  
379  $a$ , the current activation of the element. These inputs are summed and then reduced by a factor which  
380 is dependent on  $S$ , the shunting input. As in LINlinear,  $R_N$  introduces normally distributed noise to the  
381 element.

382 The output,  $y$ , of the LINexp component is given by

$$y(a) = \begin{cases} e^a - 0.9 & e^a \leq 1 + 0.9 \\ 1 & e^a > 1 + 0.9 \end{cases} \quad (9)$$

383 This component is used in the subthalamic nucleus (STN) population, as it gives a more physiologically  
 384 accurate f-I behaviour (Wilson, 2004; Bevan and Wilson, 1999; Hallworth et al., 2003) which has been  
 385 shown to allow the mapping of the basal ganglia network architecture onto an optimal decision making  
 386 model (Bogacz and Gurney, 2007).

387 The *DIMSN* and *D2MSN* components are both leaky integrators, similar to LINlinear. They differ in  
 388 that they have no shunting inhibition. They are used to model medium spiny neuron (MSN) populations  
 389 in the striatum. As they model the fact that most MSN neurons fall into two groups; those expressing D1  
 390 dopamine receptors and those expressing D2 receptors, they have a dopamine parameter that modulates the  
 391 input activation, so that their equations for  $a_{in}$  are thus:

$$a_{in}^{D1} = (0.2 + d)A + 0.01R_N \quad (10)$$

392

$$a_{in}^{D2} = (1 - d)A + 0.01R_N \quad (11)$$

393 where  $d$  is the dopamine parameter. Varying dopamine from 0 to 1 enhances the activation in the D1 model,  
 394 whereas it decreases the activation of the D2 model elements, in line with experimental observations  
 395 (Harsing and Zigmond, 1997; Gonon, 1997). Note that the equation for  $a_{in}^{D1}$  differs from that used in the  
 396 Cope-Chambers model, for which the cortico-striatal weights are multiplied by  $(1 + d)$  rather than  $(0.2 + d)$ .  
 397 A value of  $d = 0.7$

398 The equations given above are applied to each element in a population [based on the D1MSN or D2MSN](#)  
 399 [component](#). The value of the activation  $A$  (and where relevant, the shunting input,  $S$ ) is determined by  
 400 summing the weighted inputs to the population:

$$A = \sum_i w_i^{act} x_i^{act} \quad (12)$$

401

$$S = \sum_i w_i^{sh} x_i^{sh} \quad (13)$$

402  $w_i^{act}$  and  $w_i^{sh}$  are, respectively, the weights of the  $i^{th}$  activation or shunting connections [received by the](#)  
 403 [component](#);  $x_i^{act}$  and  $x_i^{sh}$  are the signals input to the activation and shunting connections.

#### 404 2.2.2 Population activity and retinotopic mapping

405 Each population of 2500 neural elements was arranged in a 50 by 50 grid, with positions on the grid  
 406 representing a retinotopic mapping similar to that found empirically both in the superior colliculus (Ottes  
 407 et al., 1986) and in visual cortex (Schwartz, 1980) and assumed in this work to persist throughout the  
 408 oculomotor system.

409 In a retinotopic mapping, the Cartesian co-ordinates of the light-sensitive cells in the retina, whose density  
 410 varies with distance from the fovea, are transformed into the Cartesian co-ordinates of the correspondingly  
 411 active cells on the colliculus. The mapping ensures that an even density of cells can be maintained in the  
 412 colliculus, but ensures that a group of adjoining, active, retinal neurons will always activate an adjoining  
 413 group of neurons on the collicular surface.

414 The mapping turns out to resemble polar co-ordinates. That is, one axis of the collicular surface specifies  
 415 the eccentricity of a retinal location (how far it is from the fovea) and the second axis specifies the rotational  
 416 angle of the retinal location; we therefore use the convention of referring to the eccentricity axis on the  
 417 colliculus as  $r$  and the rotation axis as  $\phi$ .

418 The *cortical magnification factor*,  $M(r)$ , gives the relationship between the radial eccentricity  $r$  and the  
 419 retinal neural density. As in Cope et al. (2017), we use a first-order approximation of the form for  $M(r)$   
 420 given in Rovamo and Virsu (1979):

$$M(r) = \frac{M_f}{1 + \frac{r}{E_2}} \quad (14)$$

421 The foveal magnification,  $M_f$ , is the magnification of the most central region of the retina and has a value  
 422 in the human of about  $7.8 \text{ mm}^\circ$  (Rovamo and Virsu, 1979).

423 In our model,  $M_f$  is related to  $W_{nfs}$ , the width of the retinotopic neural field,  $W_{fov}$ , the width of the  
 424 eye's field of view and  $E_2$ , the eccentricity at which the retinal density has halved by:

$$M_f = \frac{W_{nfs}}{E_2 \ln \left( \frac{W_{fov}}{2E_2} + 1 \right)} \quad (15)$$

425 Here,  $W_{nfs}$  is 50 (the side length of the 50x50 grid) and  $W_{fov}$  is set to  $61^\circ$ , a reduction from the  
 426 biophysically accurate  $150^\circ$  due to the small number of neurons in the retinotopic neural field.  $E_2$  is 2.5  
 427 (Cope et al., 2017; Slotnick et al., 2001).

428 The mapping from the retinotopic co-ordinates in the brain to rotational co-ordinates of the stimu-  
 429 lus/response was written down by Schwartz (1977, 1980) for measurements of striate cortex [visual  
 430 stimulus to electrophysiological response—Daniel and Whitteridge (1961); Talbot and Marshall (1941)]  
 431 and by Ottes et al. (1986) for superior colliculus data [electrophysiological SC stimulus to eye movement  
 432 response—Robinson (1972)]. We used the following statement of this mapping to introduce stimuli into  
 433 the ‘World’ input population of the brain model:

$$\phi = \frac{W_{nfs}}{2\pi} \arctan \left( \frac{\theta_y^t}{\theta_x^t} \right) \quad (16)$$

434

$$r = M_f E_2 \ln \left( \frac{1}{E_2} \sqrt{\theta_x^{t2} + \theta_y^{t2}} + 1 \right) \quad (17)$$

435 Note that we use  $r$  and  $\phi$  as the co-ordinates on the ‘collicular surface’. Schwartz uses  $r$  and  $\phi$  as the polar  
 436 coordinates of the retinal stimulus; Ottes et al. use  $r$  and  $\phi$  as polar coordinates for the eye movement  
 437 response; both use  $u$  and  $v$  as the Cartesian co-ordinates of the neural map. We use  $\theta_x^t$  and  $\theta_y^t$  to give Euler  
 438 rotations for the retinal target stimulus. Note also that the form of Eqns. 16 & 17 is slightly different from  
 439 that given in Ottes et al. (1986) because our  $\theta_x^t$  and  $\theta_y^t$  are not the polar co-ordinates used in that work.

440 The mapping encompasses the entire visual field; the value of  $\phi$  is allowed to vary from  $0^\circ$  to  $360^\circ$  along  
 441 its axis. Effectively, the two contralateral colliculi found in the biology are incorporated into a single,  
 442 square map, avoiding the need to carry out the kind of ‘colliculus gluing’ described in Tabareau et al.  
 443 (2007).

444 It is straightforward to show that the reverse mapping is given by:

$$\theta_x = E_2 \left( e^{\frac{r}{M_f E_2}} - 1 \right) \cdot \cos \left( \frac{2\pi\phi}{W_{nfs}} \right) \quad (18)$$

445

$$\theta_y = E_2 \left( e^{\frac{r}{M_f E_2}} - 1 \right) \cdot \sin \left( \frac{2\pi\phi}{W_{nfs}} \right) \quad (19)$$

446 where we have dropped the  $t$  superscript on  $\theta_x$  &  $\theta_y$ , as these equations transform a collicular location into  
447 rotations of the eye.

448 Fig. 3 shows the result of the mapping for a view of two cross-shaped luminances. One cross illuminates  
449 the fovea, which results in a large comb-shape of activity. The more peripheral cross produces (in FEF) an  
450 indistinct object centred at a larger value of  $r$ .

#### 451 2.2.3 Network

452 Briefly, the model consists of input from the World population (see Fig. 2, green population box)  
453 producing activity in an ‘express’ pathway to superior colliculus (purple) and simultaneously in cortex,  
454 represented here by the FEF population (grey boxes in Fig. 2). The express pathway causes short latency  
455 activity in the superficial superior colliculus, which directly innervates the deeper layers of the superior  
456 colliculus (SC\_deep). Activity in FEF generates firing in a thalamo-cortico-basal ganglia loop. The output  
457 of the basal ganglia is the substantia nigra pars reticulata (SNr) which tonically inhibits SC\_deep. If a  
458 location of activity in FEF is able to dominate selection in the basal ganglia circuit, the corresponding  
459 location in SNr will dis-inhibit and activity will build up in SC\_deep encoding the saccade end point.

460 Connections shown in red are one to one connections; dark blue projections indicate a connectivity pattern  
461 which ‘fans out’ with a 2-D Gaussian kernel; lighter blue connections from the subthalamic nucleus (STN)  
462 to SNr and globus pallidus externum (GPe) are diffuse, all-to-all connections and projections coloured  
463 green are one-to-one connections that decay towards the fovea so that foveal activity in FEF does not  
464 swamp the basal ganglia which would prevent peripheral luminances from ever being selected. Note  
465 that SC\_deep contains two recurrent connections; one is excitatory, with a Gaussian kernel mapping and  
466 the other implements tecto-tectal inhibition, which increases the inhibition between activity in opposite  
467 hemispheres of the field of view (Gian G. Mascetti and Jorge R. Arriagada, 1981; Olivier et al., 2000)  
468 helping to resolve competition between saccades to the left and right. The tecto-tectal inhibitory connection  
469 is *not* present in the Cope-Chambers model. In all other respects the model is as described in Cope et al.  
470 (2017). We have not listed the parameters of the network in tabular form here, instead, the reader is referred  
471 to the SpineML declarative specification of the model from the link given in SUPPLEMENTAL DATA.  
472 The easiest way to access this information is by using SpineCreator.

#### 473 2.3 Brainstem model

474 We implemented a saccadic burst generator (SBG) based on the connectivity outlined in Gancarz and  
475 Grossberg (1998). The SBG network for two of the model’s six channels is shown in Fig. 4. In the brainstem  
476 model, we use the word ‘channel’ to mean a set of populations of neurons which are involved in actuating  
477 a single extraocular muscle. SBG channels are arranged in pairs, actuating opposing muscles. There is  
478 one pair of channels which actuates the superior and inferior rectus muscles, causing vertical rotations  
479 of the eye in a roughly parasagittal plane (the eye moves up or down). Another pair actuates the lateral  
480 and medial rectus muscles, causing horizontal rotations of the eye. The third pair actuates the superior  
481 and inferior oblique muscles which contribute to vertical as well as oblique rotations. Activity from the  
482 output layer of superior colliculus (SC\_avg) is fed into each channel, which sums the activity it receives and  
483 processes it in populations each of a single neural element representing all the neurons in that population.  
484 Each channel of the SBG functions to create the motor neuron activations that are required to accelerate  
485 the eye in a particular direction, then hold the eye in its new position against the returning force generated  
486 by the elastic properties of the muscles. The required motor neuron activations are therefore a combination  
487 of features: a brief burst of increased activity that accelerates the eye; followed by a period of activity that

488 is less than the burst firing rate but higher than the tonic rate that exists when the eye is at the centre. This  
 489 holds the eye in its new position.

490 The SBG connectivity produces each of the these features separately, then sums them to create the desired  
 491 ‘bump and tonic’ activation time series. The input to the first population in the SBG, the long-lead burst  
 492 neurons (LLBNs), is conceived as originating from one of the deep layers of the superior colliculus. The  
 493 activity of the LLBNs are passed to excitatory burst neurons (EBNs) which, in turn, inhibit the LLBNs via  
 494 the activity of the inhibitory burst neurons (IBNs). This feedback loop has a transmission delay, which  
 495 allows activity to build up in the EBNs before the inhibition is activated and the activity is then reduced  
 496 again. This mechanism generates the ‘bump’.

497 The generation of the ‘tonic’ phase of the required time series is achieved simply by integrating the bump  
 498 over time and multiplying by a some small gain factor. This is the function of the tonic neurons (TNs).  
 499 The firing rate of the motor neuron defines the amount of force applied to the eye by that muscle. Thus,  
 500 the integral of the ‘bump’ defines how far the eye moves in that channel’s direction. The gain and delay  
 501 parameters in the LLBN-EBN-IBN-LLBN feedback loop therefore have to be tuned such that the endpoint  
 502 of the saccade is reasonably accurate. Furthermore the restoring force generated by the elasticity of the  
 503 muscles is dependent on the radial distance. The value of the new tonic firing rate, after the ‘bump’ is  
 504 dependent on the end location of the eye. If the ratio between the EBN firing rate and the TN firing rate is  
 505 not exactly correct, the eye will drift away from the saccade endpoint after the saccade has been completed.  
 506 The EBN-TN connection strength is therefore tuned such that the TN firing rate yields a stable eye position  
 507 across a range of eye eccentricities.

508 The omnipause neurons (OPNs) are tonically active and inhibit the EBNs. The activity of the OPNs is  
 509 itself inhibited by activity in the LLBNs. The purpose of this arrangement is to ensure the eye does not  
 510 move in response to neural noise.

511 Each mean activity of all the neurons in each SBG population (except the TNs) is defined by a single  
 512 leaky integrator, first order differential equation.

$$\frac{da}{dt} = \frac{1}{\tau}(y - a) \quad (20)$$

513 where  $a$  is the activation of the nucleus, and  $\tau$  is the time constant of the nucleus.  $y$  is a piecewise linear  
 514 function of the weighted sum of inputs to the nucleus and is given by

$$y(IN) = \begin{cases} 0 & IN \leq b \\ IN - b & b \leq IN \leq 1 + b \\ 1 & IN \geq 1 + b \end{cases} \quad (21)$$

515 where  $b$  is the  $IN$  axis offset.  $IN$  is the weighted sum of inputs to the nucleus and is given by,

$$IN = \sum_m^M w_{mn} a_m \quad (22)$$

516 where  $a_m$  is the activation of the  $m^{th}$  afferent nucleus.  $w_{mn}$  is the connection strength between the  $m^{th}$   
 517 afferent nucleus and the current nucleus. The activity of the TNs are defined as

$$\frac{da}{dt} = \frac{1}{\tau} y \quad (23)$$

518 with an identical piecewise linear transfer function as the other SBG populations.

## 519 2.4 Biomechanical eye

520 The output signals of the brainstem's **motoneuron (MN) populations** are used to drive the biomechanical  
 521 model. **The MN output signal in each brainstem channel is normalised in the range [0 1] and represents the**  
 522 **mean firing rate of the neurons that innervate the extraocular muscle for that channel.** The biomechanics  
 523 are used not only to get tangible feedback on the simulated saccades including motion trajectories, but  
 524 to add one more modelling dimension related to the inertial properties of the eye plant including muscle  
 525 properties.

526 The biomechanical eye model, implemented using the OpenSim framework (Seth et al., 2011), is  
 527 anatomically represented by a sphere of uniform mass distribution. The diameter of the eye is 24 mm for  
 528 adults, with small variations between individuals; the mass of the eye is 7.5 grams. The eyeball is actuated  
 529 by six extraocular muscles (EOMs). The EOMs are arranged in three pairs forming a cone inside the orbit  
 530 with the apex being located inside the cranium in a tendonous ring called the annulus of Zinn. An important  
 531 feature of the oculomotor system which greatly affects its overall behavior is the existence of dynamic  
 532 EOM pulleys. Their role is to guide the pivot point of the EOMs. In our model, a pulley for each EOM has  
 533 been modeled by a point on the orbit whose location depends on the current eye orientation.

534 An illustration of the biomechanical eye model is given in Figure 5, while Figure 5 depicts the head  
 535 model used in the proposed framework.

536 Two types of muscle models of different complexity are supported. The first models muscles using linear  
 537 path actuators. This simplistic model of ideal muscles can be easily integrated with high level brain models.  
 538 As described above the muscles are wrapped around the eye. The more complex model supported is based  
 539 on the Thelen model (Thelen, 2003) that is also supported by OpenSim and implements Hill-type muscles.  
 540 It includes realistic muscle wrapping geometric entities of the muscle fibers, while it accommodates for  
 541 both activation and contraction dynamics. The dynamics of muscular forces can be split into: 1) The  
 542 elasticity of the muscles. 2) A delay between the onset of the afferent excitatory signal and the actual  
 543 muscle contraction, caused by the transmission time of the action potentials and by the necessary calcium  
 544 release at the muscle fibres.

545 The force applied by EOMs is controlled by an excitatory signal supplied by motoneurons in the brainstem.  
 546 The neural drive to produce a saccadic eye movement can be characterized by a pulse component to  
 547 overcome the viscoelasticity of the orbital plant, a step component to stabilize the eye in the new position,  
 548 and a slide component that models the gradual transition between the pulse and step.

549 Passive forces due to the fatty tissues inside the eye orbit also affect eye dynamics. Their role is critical in  
 550 eliminating the influence of head and body movements. We incorporated a custom torque,  $t$ , which acts  
 551 like a rotational spring-damper apparatus, resisting eyeball movements. It has elastic and viscous properties  
 552 governed by  $t = -K\mathbf{R} - C\dot{\mathbf{U}}$  where  $\mathbf{R}$  is the eye's orientation and  $\mathbf{U}$  is its angular velocity.  $K$  and  $C$  are  
 553 constants. A fuller description of the biomechanical model can be found in Papapavlou and Moustakas  
 554 (2014).

## 555 2.5 Model development framework

556 The Cope-Chambers model was originally developed to run on the BRAHMS model execution framework  
557 (Mitchinson et al., 2010; Mitchinson and James, 2015). To run a BRAHMS model, the researcher must  
558 develop *BRAHMS components* for the various neural elements. A BRAHMS component is a program-  
559 matically coded implementation of the behaviour of the component. It may have an arbitrary number of  
560 inputs and outputs and may be written in C, C++, Python or MATLAB. The Cope-Chambers model's  
561 components were hand written in C++ and MATLAB. A BRAHMS *SystemML* file describes how the  
562 different components connect together and how data is passed between them (Mitchinson et al., 2010). The  
563 main BRAHMS program first reads the SystemML file, then dynamically loads all the required components  
564 before executing the system.

565 In the current work, the Cope-Chambers model was reproduced using the declarative SpineML markup  
566 language (Alex Cope and Paul Richmond, 2014; Richmond et al., 2014), with the help of the graphical  
567 SpineML model editing software called SpineCreator (Cope et al., 2015, 2016). SpineML, which is a  
568 development of the NineML specification (INCF Task Force on Multi-Scale Modeling, 2011), describes  
569 neural populations and their projections in a highly structured format in which neuron bodies, pre- and post-  
570 synapses are described in terms of *SpineML components*. These are similar to the components provided by  
571 BRAHMS, but in this case, the components are an XML description of the functionality of the component,  
572 rather than a programmatic implementation, with one XML file per component. A SpineML *network layer*  
573 file then describes which components are used in the model, and how they are connected together. Finally,  
574 a number of SpineML *experiment layer* files specify how the model described in the network layer can be  
575 executed. In the experiment layer, the execution duration and timestep can be specified, along with input  
576 conditions, connection lesions and component parameter updates. A description of SpineML is given in  
577 Richmond et al. (2014); the definitive definition is found in the schemas (Cope et al., 2014). SpineCreator,  
578 in its rôle as a graphical editor for the SpineML format, was used to generate the SpineML files describing  
579 the model. It was also used to generate the diagrams of the model.

580 As a declarative format for model specification, SpineML is agnostic about how the model is executed. A  
581 number of simulation engines can be utilised, including DAMSON (Richmond, 2015), GeNN (Nowotny,  
582 2011; Nowotny et al., 2014) and BRAHMS (used here). The simulation engine incorporating BRAHMS is  
583 called SpineML\_2\_BRAHMS (Cope and James, 2015). SpineML\_2\_BRAHMS is a collection of XSLT  
584 stylesheets which first generate and compile C++ BRAHMS components from the SpineML component  
585 layer description files. SpineML\_2\_BRAHMS then uses the SpineML network and experiment layer files  
586 to generate a BRAHMS SystemML description of the model. Finally, SpineML\_2\_BRAHMS executes the  
587 model, now described entirely as a BRAHMS system, via a call to the BRAHMS binary. A number of  
588 additional hand-written components are present in SpineML\_2\_BRAHMS providing the inputs (constant  
589 inputs, time-varying inputs, etc) which the modeller specifies in the experiment layer.

590 In addition to the brain model components, all of which are code-generated using SpineML\_2\_BRAHMS as  
591 described above, two hand-written components are integrated into the model: The biomechanical eye model  
592 and a sensory input component. The sensory input component takes the eye's rotational state and the state  
593 of the experimental luminances and projects a retinotopic activity map into the brain model. Both of these  
594 BRAHMS components were hand-written in C++. To incorporate these components into the SpineML  
595 model, a SpineML\_2\_BRAHMS *external.xsl* file was used. The external.xsl file scheme for incorporating  
596 external BRAHMS components into a SpineML model was a new SpineML\_2\_BRAHMS feature motivated  
597 by the current work. Fig. 6 shows the workflow, in which the model specification files (blue box - a

598 combination of SpineML files and C++ code), are processed (green box) into a BRAHMS system (red  
 599 box).

600 Finally, numerical integration of the biomechanical eye model is based on the Kutta-Merson integration  
 601 method.

## 602 2.6 Integrating the models and closing the loop

603 The Cope-Chambers model closed its loop by passing the centroid of activity in SC\_deep (once it had  
 604 surpassed a threshold) back to the code that controlled the world, which would then use this location to  
 605 instantaneously change the model's view of the world. In our extended model, it was necessary to connect  
 606 the output of the brain model back to its input via the saccadic burst generator model and the biomechanical  
 607 eye. The resulting state of the eye, rather than the centroid of the superior colliculus, was used to compute  
 608 the input to the brain, given the luminances visible in the world.

609 Thus, the information flow in the model is as follows: Luminances in the world have their locations  
 610 computed in the eye's frame of reference, based on the rotational state of the eye. The locations of the  
 611 luminances on the retina are transformed into a retinotopic co-ordinate system which determines the  
 612 activity in the 'World' population (named to mean the 'world as the eye sees it', rather than the world  
 613 frame of reference) which is the input for the brain model. The target luminance for a saccade is selected,  
 614 as described earlier, via cortical and sub-cortical loops through the basal ganglia model and activity for  
 615 the winning end-point builds up in the deep layer of superior colliculus. This activity excites activity  
 616 in the correct proportions within the 6 channels of the saccadic burst generator whose output state, the  
 617 motoneurons send a rate-code signal (normalised between 0 and 1) into the biomechanical eye model. The  
 618 rotational state of the eye model is fed back to participate in the computation of the retinotopic luminance  
 619 activity in 'World', completing the loop.

620 A number of studies have considered the form of the connection between the deeper layers of the superior  
 621 colliculus and the saccadic burst generator (Van Gisbergen et al., 1985; Ottes et al., 1986; Waitzman et al.,  
 622 1991; Groh, 2001; Arai et al., 1994; Goossens, 2006; Tabareau et al., 2007; van Opstal and Goossens,  
 623 2008; Goossens and van Opstal, 2012), which has become known as the spatial temporal transform (STT).  
 624 The spatial aspect of the transform is thought to be implemented by a weight-mapping (Tabareau et al.,  
 625 2007; Arai et al., 1994). Although there is no definitive experimental proof for such a mapping, there  
 626 exists evidence for spatially variable synapse density (Moschovakis et al., 1998; Herrero et al., 1998) and  
 627 connection density (Grantyn et al., 2002) and we therefore adopt the idea. Arai and co-workers trained a  
 628 20x20 neural network model of the superior colliculus to discover the weight map under the assumption  
 629 of 2D Gaussian activation profiles (Arai et al., 1994)—that is, they assumed that the activity in superior  
 630 colliculus for any saccade was a size-invariant 2D Gaussian hill of activity. The training approach of  
 631 Arai et al. (1994) was not feasible in this study due to the length of time required to run our model and  
 632 its stochasticity, which meant multiple runs of the model were necessary in order to generate output  
 633 statistics. Tabareau et al. (2007) wrote down a theoretical form of the weight map, obtained by inverting the  
 634 mapping of Ottes et al. (1986) and the assumption of invariant 2D Gaussian activity profiles in SC, which  
 635 is equivalent to:

$$w(r, \phi) = i e^{jr} \sin(l\phi + k) \quad (24)$$

636 where  $r$  and  $\phi$  are co-ordinates on the collicular map and  $i, j, k$  and  $l$  are parameters of the function  
 637 (compare with Eq. 3 of Tabareau et al. (2007)). As they found it closely resembles the results of Arai et al.  
 638 (1994), and it is a simple formulation, we considered it as the means to generate the six weight maps in our

639 own model. One barrier to the use of this weight map was the Cope-Chambers model's violation of the  
 640 *invariant integral hypothesis*. This states that the number of spikes emitted by a neural element during a  
 641 saccade (or in our model, the integral of the neuron's output during the saccade) should be a function only  
 642 of its position within the hill of collicular activity. That is, for any time-dependent hill of activity  $\mathcal{A}(\mathbf{z}, t)$  at  
 643  $\mathbf{z} = (r, \phi)$  on the collicular surface, the integrated activity  $A_{\mathbf{x}}$  in an element at a vector  $\mathbf{x}$  away from  $\mathbf{z}$  is

$$A_{\mathbf{x}} = \int_t \mathcal{A}(\mathbf{z} - \mathbf{x}, t) dt \quad (25)$$

644 which is invariant for all  $\mathbf{z}$ . This requirement is fulfilled by spatially invariant 2D Gaussian profiles, whose  
 645 time-course (how quickly they grow and then diminish) is always the same.

646 However, the very mapping on which the Tabareau et al. (2007) result is based leads to a very *variant*  
 647 activity profile in the SC\_deep layer of the Cope-Chambers model. A luminance of a given size which  
 648 excites activity near to the fovea causes activity in a large number of neurons in each retinotopic layer,  
 649 whereas activity far from the fovea excites a much smaller region. This effect is clearly demonstrated in  
 650 Fig. 3 for equal sized targets both on and distal from the fovea.

651 To understand the need for this invariance, consider the effect of a 2D Gaussian hill in SC\_deep which  
 652 elicits a successful horizontal saccade of 10°. Activity from the 2D Gaussian, passing through the weight  
 653 maps will excite the superior and inferior rectus channels by an equal, balanced amount, so these cancel out,  
 654 allowing the eye movement to be horizontal. The amount of activation passed to the lateral rectus muscle  
 655 results from a convolution of the Gaussian and the exponential component of the weight map relationship  
 656 in Eq. 24. If the Gaussian hill now appears further along the collicular surface, coding for a 20° saccade,  
 657 and also becomes smaller, we can still argue that the vertical component signals to superior/inferior rectus  
 658 muscles will cancel out, and we could imagine that the exponential component of Eq. 24 is correctly  
 659 parameterised to compensate for the smaller hill. However. Now consider a 2-D Gaussian hill which codes  
 660 for a 10° saccade which is 'up, and to the right' in equal proportions. That means that the hill will sit on  
 661 the boundary between the weight maps for the 'up', and the 'right' muscles. Now, if the hill moves to  
 662 the  $r = 20^\circ$  location on the colliculus, and also reduces in size, it will excite only the periphery of the  
 663 sine; the exponential increase of the map along  $r$  is not guaranteed to compensate for the reduction in the  
 664 convolution of the Gaussian hill and the sinusoidal component of the weight map.

665 This led us to hypothesise that the retinotopic mapping to the SBG be preceded by an associated widening  
 666 projection field such that the hill of activity in a 'final' deep layer of superior colliculus is invariant with  
 667 position on the map. There are a number of locations in the system in which this widening projection  
 668 field could exist. It could be implemented in the projections between the retinal populations and the  
 669 superficial layer of SC along with the projection between the World and the FEF population. However,  
 670 this would affect activity within the basal ganglia of the model, contradicting a result in Cope et al. (2017)  
 671 which explains the 'hockey stick' profile for saccade latency as a function of saccade eccentricity. Instead,  
 672 we suggest that a widening projection field is encoded within the superior colliculus itself, a complex,  
 673 multi-layered structure which could quite plausibly support such a function. Indeed, such widening activity  
 674 can be seen in the stimulation experiments in Vokoun et al. (2010) and Vokoun et al. (2014). In Ghitani  
 675 et al. (2014), from the same research group, evidence is presented for an excitatory and widely projecting  
 676 pathway from the stratum griseum intermediale (equivalent to our SC\_deep) to the more superficial layers  
 677 stratum opticum and stratum griseum superficiale. Although this pathway is a 'wide' projecting field,  
 678 the experiments do not indicate whether the projection widens along the rostral-caudal axis of the SC.  
 679 Bayguinov et al. (2015) presents evidence for another projecting field within SC whose connectivity pattern

680 *does change along the rostral-caudal axis. This projection is inhibitory in nature. Although neither of*  
 681 *these results precisely match the widening, excitatory projection field hypothesised here, they do indicate*  
 682 *that such connection patterns are plausible.* Although in this work we do not model the SC in detail, we  
 683 extended the model with a third functional layer named SC\_deep2, shown in Fig. 7(b) (Cope-Chambers has  
 684 only the two layers SC\_sup and SC\_deep). We introduced a widening projection based on a Gaussian  
 685 projection field whose width,  $\sigma(r)$  varies in inverse proportion to the magnification factor,  $M(r)$ , given in  
 686 Eq. 14 according to:

$$\sigma(r) = \frac{m_\sigma}{M(r)} - \frac{m_\sigma}{M^0} + \sigma_0 \quad r > r_0 \quad (26)$$

687  $m_\sigma$  is a scalar parameter which determines the ‘magnitude of the widening’.  $M^0$  is the ‘starting’ magni-  
 688 fication factor; within the foveal region ( $0 \leq r \leq r_0$ ), the projection field is not allowed to widen and  
 689 so

$$\sigma(r) = \sigma_0 \quad r \leq r_0 \quad (27)$$

690 which makes  $\sigma_0$  the width of the Gaussian projection field within the foveal region. (Note that the value  
 691 chosen for the width of the foveal region,  $r_0$  is not identical to the foveal shift parameter used in the  
 692 *DecayingAtFovea* projections into striatum.) The *Widening Gaussian* projection weight,  $w(r, d)$  is then  
 693 computed as:

$$w(r, d) = e^{-\frac{d^2}{2\sigma(r)^2}} \quad (28)$$

694 where  $d$  is the distance between the source and destination elements in the collicular plane.  $m_\sigma$  was set to  
 695 50,  $\sigma_0$  was 0.3,  $M^0$  was 12.43 and  $r_0$  was 20.

696 A further issue regarding the use of the theoretical weight map in Tabareau et al. (2007) was that it does  
 697 not consider the existence of the oblique extraocular muscles. There is evidence that only two dimensional  
 698 information is encoded in superior colliculus (Wurtz and Goldberg, 1972; Hepp et al., 1993; Van Opstal  
 699 et al., 1991), but the eye is actuated by six extraocular muscles. In order to find out a possible form for the  
 700 input to the oblique muscles we carried out a training process which depended on a centroid computation in  
 701 SC\_deep and was designed to maintain a null torsional eye rotation for all saccade end-points. For the four  
 702 rectus muscles, the resulting weight map solutions resembled those found by Arai et al. (1994). The trained  
 703 maps for the oblique muscles had a form very close to those for the inferior and superior rectus channels,  
 704 but with a smaller magnitude. The inferior oblique map resembled the superior rectus map and the superior  
 705 oblique map resembled the inferior rectus. When parameterising the theoretical weight maps, we set the  
 706 inferior/superior oblique maps to be 1/10<sup>th</sup> of the superior/inferior rectus maps, respectively. Interestingly,  
 707 this suggests that there is a built-in synergy between the vertical and oblique channels in the eye, although  
 708 the results will show there is some systematic change in the oblique error with saccade end-point location.

709 Tabareau et al. (2007) give a formulation for the weight maps in which it is possible to project both a  
 710 positive and a negative weight. In our model, all projections from SC\_deep are excitatory. This means that  
 711 each channel has a weight which follows the form:

$$w(r, \phi) = i e^{jr} \sin \left( \frac{2\pi\phi}{W_{nfs}} + k \right) \quad (29)$$

712 where  $i, j$  and  $k$  are per-channel parameters for the weight maps.  $k$  is determined by the mapping. Only the  
 713 positive part of the sine is utilised.  $i$  and  $j$  are parameters to be found.

The saccadic burst generator model was originally conceived with the assumption of a step input, which returns to zero activity at a suitable time to curtail the saccade and avoid staircase saccades (Gancarz and Grossberg, 1998). In our model there is no such mechanism to reduce activity in SC\_deep, and elsewhere. Although a successful, accurate saccade towards a target luminance will remove the excitation which caused the activity in SC\_deep by bringing the target luminance within the masked, foveal region, the activity in SC decays too slowly to avoid additional saccadic movements. We found it necessary to hypothesise an inhibitory feedback mechanism from the SBG to the brain model. This is shown in Fig. 4, which indicates how the output from the inhibitory burst neurons (IBN) of the SBG model are used to feed back an inhibitory signal to the SC\_deep, thalamus and FEF populations in the brain model, resetting them ready for the next saccade. There is evidence for inhibitory projections to SC from the propositus hypoglossi nucleus (Corvisier and Hardy, 1991), which lies within the brainstem, upstream from motoneurons, and has been shown to encode eye velocity (Dale and Cullen, 2013).

The output signals from the six channels of the SBG were connected to the six motoneuron inputs of the biomechanical eye. The signal was normalised; a value of 1 meaning that all the motoneurons in the output population were firing at their maximum rate and the force exerted by the relevant extraocular muscle was maximal. Channels innervated extraocular muscles as follows: Up: superior rectus; Down: inferior rectus; Right: medial rectus; Left: lateral rectus; Z+: superior oblique; Z-: inferior oblique. Because the medial rectus induces a rightward rotation of the eye, our single virtual eye is a *left* eye. The OpenSim implementation of the biomechanical eye was ‘wrapped’ (in the software sense) in a BRAHMS component. This made it possible to integrate the OpenSim model into the BRAHMS framework. The wrapper ensured that the input and output signals were correctly transferred and, importantly, handled the disparity in the solver timesteps used in the OpenSim model (25 ms) and the neural model (1 ms). This was achieved by having the BRAHMS wrapper create a separate thread to run the OpenSim model. The BRAHMS wrapper component was called on each 1 ms timestep, receiving the instantaneous activations from the motoneurons in the SBG. These activations, and the current simulation time, were written into a shared memory area, accessible by the OpenSim thread. Running independently, the OpenSim thread would update its inputs (using the most recent values in the shared memory area) whenever the simulation time had increased by 25 ms. It would then recompute its outputs (the rotational state of the eye) and write these into the same shared memory. The BRAHMS wrapper would update its outputs whenever they were changed in the shared memory by the OpenSim thread. A direct connection of the six outputs of the BRAHMS eye model component to the six inputs of the worldDataMaker BRAHMS component was specified in the SpineML\_2\_BRAHMS external.xsl file.

The eye model outputs its rotational state at each timestep. The rotational state is used to compute the view of the world in the eye’s frame of reference. To simplify the calculation, the luminances exist on a spherical surface at the centre of which is the eye. A hand-coded BRAHMS component called worldDataMaker computes the projection of the luminances into the eye’s frame of reference and then converts this representation into a retinotopic map to pass into the brain model. The input to the brain model is thus able to change continuously, on every timestep, rather than in a step-wise fashion when a saccade occurs, as in the Cope-Chambers model.

In the worldDataMaker BRAHMS component, the rotational state of the eye was used to construct Euler rotation matrices which transformed between the world’s frame of reference and the eye’s frame of reference. The worldDataMaker component received a specification of the world luminances in a JSON file called luminances.json at the start of each simulation. luminances.json specified the position, shape, size, luminance, appearance time and disappearance time of an arbitrary number of luminances. With this

758 information, the instantaneous rotational state of the eye and the parameters of the retinotopic transform, it  
759 was able to compute the instantaneous input to the brain model.

760 The final models, on which the results of this paper are based are named ‘TModel3’, ‘TModel4’ and  
761 ‘TModel5’. Descriptions of these, and earlier versions of the model can be found in the code repository  
762 given in SUPPLEMENTAL DATA.

### 3 RESULTS

#### 763 3.1 Weight maps

764 We found the best parameters for the exponential in Eq. 29 ( $i$  and  $j$ ) by a manual tuning process. After  
765 selecting values for  $i$  and  $j$  in either the horizontal or vertical/oblique channels, we ran the model 6 times  
766 at each of 8 target eccentricities ( $7^\circ$ – $14^\circ$ ) which were purely in the direction of the newly parameterised  
767 channel. The training saccades were produced as described below in Sect. 3.3, with the same fixation  
768 and target luminances (crosses of magnitude 0.2 and 0.3) but with the fixation offset and target onset  
769 occurring at 0.2 s. We measured the end-point of the saccade by detecting the location at which the saccade  
770 velocity had dropped below 0.005 of its peak. We iterated until the mean saccade endpoint plotted versus  
771 target was close to the ideal straight line—see Fig. 8(a) & (b). We applied the same parameters to both  
772 directions of each channel;  $i_{up} = i_{down} = 0.00195$ ,  $j_{up} = j_{down} = 0.075$ ,  $i_{left} = i_{right} = 0.0016$  and  
773  $j_{left} = j_{right} = 0.067$ .

774 The resulting weight maps (where the oblique maps are 1/10<sup>th</sup> of the vertical maps, as described earlier)  
775 are shown in Fig. 9. First, recall that the  $r$  axis of the neural surface corresponds to the amplitude of a  
776 saccade and the  $\phi$  axis indicates the polar direction of the saccade, as described in Sect. 2.2.2 and Fig. 3.  
777 Fig. 9(a) shows the weight map for the muscle which rotates the eye to the left. As we modelled a left  
778 eye, this actuates the lateral rectus muscle. The exponential rise of Eq. 29 [for experimental evidence, see  
779 Figs. 7 & 8 of Herrero et al. (1998)] is seen in the  $r$  direction; as  $r$  increases, so the connection strength to  
780 the SBG channel rises exponentially. The connection strength is greatest along the centre line, for a value  
781 of  $\phi$  which corresponds to a purely leftward movement. Note that  $\phi$  is presented in neural coordinates,  
782 and not in degrees or radians;  $1 \leq \phi \leq 50$  corresponds to a range of  $0^\circ$  to  $360^\circ$ ;  $\phi = 38.5$  corresponds to  
783 movements left. The connections strength drops away sinusoidally as  $\phi$  moves away from the centre line at  
784  $\phi = 38.5$ . In regions of the map for which there is no leftward movement, that is, in the half of the map  
785 which corresponds to any movement with a rightward component, the ‘left’ weight map is 0. Fig. 9(d)  
786 shows the weight map for rightward movements, actuating the medial rectus muscle of the eye. The line of  
787 maximum connection strength is along  $\phi = 13.5$ . The map is a mirror of Fig. 9(a), reflected about the line  
788  $\phi=26$ . The ‘left’ and ‘right’ weight maps are orthogonal; the non-zero region of the ‘left’ map is zero in the  
789 ‘right’ map and vice versa. Fig 9(b) & (d) show the weight maps for downward and upward eye movements;  
790 the ‘down’ map activates the SBG channel for the inferior rectus muscle, the ‘up’ map activates the superior  
791 rectus. Note that ‘down’ is not orthogonal either to ‘left’ or ‘right’ because a saccade down and left is  
792 achieved by simultaneously activating both the lateral and inferior rectus muscles. However, the ‘up’ map  
793 is orthogonal to the ‘down’ map and spans the edges of the surface where  $\phi$  rolls over from 1 to 50. The  
794 line of maximum connection strength for the ‘up’ map is along  $\phi = 1$ ; for ‘down’  $\phi = 26$ . Based on the  
795 training described in Sect. 2.6, the maps driving the superior oblique (‘Z+’) and inferior oblique (‘Z-’)  
796 muscles were set to 1/10<sup>th</sup> of the ‘down’ and ‘up’ maps.

### 797 3.2 Saccade accuracy

798 In Fig. 8, we showed the result of running the model to targets located on the principle axes, on which  
799 the model was trained. We then simulated single saccades to targets in one hemifield of the eye's field of  
800 view, with eccentricities between  $6^\circ$  and  $14.5^\circ$ . As in the training, we ran the simulation 6 times for each  
801 target,  $\theta^t = (\theta_x^t, \theta_y^t, 0)$  to obtain mean saccade end-points. Fig. 10 shows saccade accuracy results for an  
802 entire hemifield in the naïve model which passed the output of SC\_deep directly to SBG via the weight  
803 maps. The ratio of the magnitude of the error vector to the magnitude of the target vector is plotted using a  
804 colour map. This ratio is shown for the full, three dimensional error vector in Fig. 10(a) and for the  $x$ ,  $y$   
805 and  $z$  components in Figs. 10(b)–(c). Inspection of Fig. 10(a) shows that the end-point error is minimal  
806 along the principle axes ( $\theta_x^t = 0$  or  $\theta_y^t = 0$ ) and maximal near the  $45^\circ$  oblique targets (blue lines) with the  
807 end point error as high as 80% of the programmed saccade magnitude. The  $x$  component error map in  
808 Fig. 10(b) shows the same trend, mirrored about the 'Target X' axis, whereas the  $y$  and  $z$  component errors  
809 are, relatively, much smaller. Because the  $x$  component of the error is clearly contributing to end point  
810 errors which would not be considered 'on target', especially for oblique saccades, we considered the effect  
811 of the non-uniform size of the hill of activity in SC\_deep.

812 In our model, the location, *size* and shape of activity in FEF, the basal ganglia, thalamus and superior  
813 colliculus is eccentricity dependent, in line with the retinotopic mapping stated by Ottes et al. (1986). More  
814 eccentric targets generate reduced activity, because fewer retinal neurons are excited far from the fovea.  
815 Cope et al. (2017) showed that this relationship can explain increased saccadic latencies for distal targets,  
816 resulting from reduced activity in the decision making circuitry of the basal ganglia. However, the notion  
817 that activity in superior colliculus is eccentricity-dependent conflicts with the result of Tabareau et al. (2007),  
818 who showed that an invariant hill of activity was required if this complex logarithmic weight mapping was  
819 to be used to drive a two-degree-of-freedom saccadic burst generator, and also with experimental findings,  
820 which do not show significant eccentricity dependence, at least in the burst layer (Anderson et al., 1998).

821 To bring our model in line with these results, whilst maintaining the eccentricity dependent activity in  
822 basal ganglia, we hypothesised that a 'widening projection' exists between two maps in superior colliculus.  
823 As described in Sect. 2.6, there is now experimental evidence for similar projections (Ghitani et al., 2014;  
824 Bayguinov et al., 2015) making this a plausible suggestion. Activities in one SC\_deep layer remains  
825 eccentricity-dependent, with loops back to thalamus and cortex and through basal ganglia. This activity  
826 is then fed through a projection, which applies a Gaussian projection field, whose width increases with  
827 increasing stimulus eccentricity according to Eq. 28. The activity in this second SC\_deep layer is then  
828 fed to the weight maps of the SBG. This model was called 'TModel4'. TModel4 was parameterised such  
829 that its horizontal and vertical error was similar—so that its equivalent of Fig. 8 showed a similar sum of  
830 squares error.

831 Figs. 11(a)–(d) show the percentage errors for TModel4. First of all, note that the error magnitudes  
832 are much smaller. The mean errors are smaller for every axis. The largest errors produced by the model  
833 are approximately 15%, which are within the boundaries of what some authors have suggested would be  
834 regarded as an accurate saccade (McPeek and Keller, 2002; McPeek, 2006). The magnitude of the largest  
835 error vector is approximately  $1.5^\circ$ .

836 This result indicates that the exponential part of the Ottes et al. weight map from SC to the SBG cannot on  
837 its own compensate for the eccentricity-dependent size of the hill of activity. The introduction of a widening  
838 projection field substantially improves the mean accuracy of saccades across the field of view. We therefore  
839 suggest that the transformation between retinotopically mapped activity, and eccentricity-independent

840 activity width occurs within the superior colliculus and works alongside a simple, monotonically increasing  
841 weight map between SC and the SBG channels.

### 842 3.3 Single saccades

843 Having finalised the model by setting the weight maps, we then proceeded to exercise the model  
844 (TModel4), starting with saccades to a single target; prosaccades. Fig. 12(a) shows 9 representative  
845 saccades to a single target luminance. Initially, the eye had rotational state  $\theta_x = \theta_y = \theta_z = 0$  with  
846 its fovea directed at a fixation luminance cross (span 6°, bar width 2°) of magnitude 0.2 (in arbitrary  
847 units). At a simulation time of 0.4 s, the fixation luminance was set to 0 and a target luminance cross  
848 of the same dimensions as the fixation but with magnitude 0.3 was illuminated at one of the 9 different  
849 locations, marked by crosses in Fig. 12(a). The resulting trajectories are plotted, with colour indicating the  
850 relationship between trajectories and target crosses. The approximate end-point error is visible in this figure,  
851 although the last point in each trajectory is the saccade position at 0.8 s and not the velocity-based end-point  
852 described above. Figs. 12(b) and (c) show the rotational components of the blue and red trajectories in  
853 Fig. 12(a) along with the target and fixation luminance values. Rotations are the eye's Euler rotational  
854 components in the world frame of reference.

### 855 3.4 Saccade Latencies

856 To verify that our implementation of the brain model has the same functionality as that reported in Cope  
857 et al. (2017), we investigated the effect on saccadic response times of: target eccentricity; and any gap or  
858 overlap between fixation off-time and target on-time. We showed that the full model reproduces the 'hockey  
859 stick' shape shown in Fig. 7 of Cope et al. (2017) and discovered in experimental data (Reulen, 1984) for  
860 horizontal [Fig. 13(a)], vertical [Fig. 13(b)] and oblique saccades (not shown). The latency increases with  
861 eccentricity far from the fovea because the retinotopic mapping reduces the activity in the basal ganglia for  
862 more eccentric targets (see Fig. 3). Closer to the fovea, the *effect of* the foveal mask *on* the activity in FEF  
863 again leads to reduced input into the basal ganglia and an increased time to achieve disinhibition in SNr.

864 Fig. 13(c) shows latencies achieved when varying the time between fixation offset and target onset. This  
865 is termed the *gap condition*; and is represented by a scalar value which, if positive, refers to a gap between  
866 fixation offset and target onset, and when negative, signifies an overlap, with the fixation luminance  
867 persisting past the time at which the target is illuminated. A negative gap is also termed an *overlap*. Again,  
868 we verify the behaviour presented in Cope et al. (2017), explained as resulting from the inhibition of  
869 the cortico-thalamic loop by SNr. In the gap condition, when the fixation luminance is removed, activity  
870 in STN immediately begins to decay, allowing SNr activity to reduce and thereby reducing inhibition  
871 on thalamus, allowing the target luminance to build up quickly in FEF, thalamus and through the basal  
872 ganglia's striatum and SNr. The shape of the curves in Fig. 13(c) matches the results in Cope et al. (2017)  
873 for target luminances of 1 and 0.6; for overlaps longer than 100 ms (gap < -100 ms), the latency becomes  
874 constant; the saccade is programmed whilst the fixation is present, with the target luminance inducing  
875 sufficient activity in striatum to 'break through' the SNr inhibition caused by the fixation. If the target  
876 luminance is reduced to 0.3, the balance is altered in favour of the fixation and the latency vs. gap becomes  
877 approximately linear and equal to the overlap time plus around 100 ms.

878 Fig. 13(d) shows the effect of the dopamine parameter on saccade latencies in gap, step and overlap  
879 conditions. In general, the effect of decreasing the dopamine parameter was a smooth, monotonic and  
880 undramatic increase in saccade latency. However, the data for the overlap condition with a target luminance  
881 which was 3 times as bright as the fixation luminance was more interesting. Here we see a transition around

882 a dopamine value if 0.7. Below this value, the basal ganglia is not able to select the target luminance until  
883 the fixation is removed, reducing the excitatory drive from STN to SNr, and consequently the inhibition  
884 from SNr to the thalamo-cortical loop. For the target luminance 0.6, 0.7 dopamine allows the basal ganglia  
885 to select sufficiently well so that the target can build up in the thalamo-cortical loop, in spite of the fixation  
886 overlap.

887 The relationship between latency and the target luminance is given in Fig. 13(e). This shows latency for a  
888 100 ms gap, step and 100 ms overlap conditions for a given fixation luminance of 0.2, and a horizontally  
889 located target at  $\theta_y^t = -10^\circ$ . For the gap condition, we see very short latencies for luminances of about  
890 0.75 and above. Finally, the activity driving these express saccades is initiated by high firing rates in the  
891 superficial layer of SC (SCs), which then drives activity in thalamus and through the basal ganglia. A  
892 gradual transition from express saccades to reflexive saccades is observed as the contribution of the SCs  
893 becomes weaker and the drive from FEF into the thalamo-cortical loop becomes necessary to elicit a  
894 saccade. A similar gradual transition, albeit for higher latencies is seen for the step condition. At higher  
895 target luminances, the SCs has a greater effect on the activity in the thalamo-cortical loop. However, the  
896 activity in STN caused by the fixation luminance increases the latency at all luminance values compared  
897 with the gap condition. The overlap condition leads to increased latencies for luminances below 2.5, but  
898 meets the step condition above this value, at which the 0.2 fixation luminance appears to have a negligible  
899 effect on the system.

### 900 3.5 Saccade sequences

901 We now present results derived from the fully parameterised and integrated model; where we took  
902 advantage of the fact that it is a closed loop system. This allowed us to present sequences of target  
903 luminances and allow the model to direct its fovea at the most salient target.

#### 904 3.5.1 Out & return

905 We investigated the behaviour of the model for saccade sequences. In one experiment, we illuminated  
906 a fixation cross from 0 s until 0.4 s, followed by a target at  $(0, -10^\circ)$  from 0.4 s until 0.8 s. Finally, the  
907 fixation was again shown from 0.8 s until the end of the simulation at 2 s. This induced a saccade to a  
908  $10^\circ$  eccentricity, followed by a return saccade back to the null point. We noticed some irregularities in  
909 the return saccades, which were accurate, but had a significant overshoot. More perplexingly, if the target  
910 was switched repeatedly between  $0^\circ$  and  $10^\circ$ , second and subsequent outward saccades also showed this  
911 overshoot. We found that the cause of these irregularities was the lack (in ‘TModel4’) of any mechanism to  
912 reset the tonic neurons in the SBG after the first saccade. This resulted in TN activity in the left channel  
913 and also in the right channel. Interestingly, this ensured that, at least for a few, consecutive out-and-return  
914 saccades, the saccade accuracy was accidentally relatively good, with trajectories resembling experimental  
915 data (Bahill and Stark (1979), p. 6). Had the return accuracy not been so accurate, we may have noticed the  
916 lack of a tonic neuron reset mechanism and corrected this oversight earlier. Such a mechanism is indeed  
917 proposed and included in the connectivity of the Gancarz and Grossberg (1998) model. We implemented  
918 this feature by adding an additional inhibitory input to the ‘integrator’ component of TModel4, driven  
919 by the contralateral EBN population, naming the new model ‘TModel5’. Now, when the eye is directed  
920 towards an eccentric target which is then exchanged with a target at the null point, the EBN activity toward  
921 the null point will tend to extinguish the TN activity which was holding the eye at the eccentric position.  
922 We verified that none of the single saccade results were affected by this modification.

923 Fig. 14 shows the outward and return trajectories produced by the experiment with the TN reset mechanism.  
924 Panel (a) shows the  $x$  and  $y$  rotation trajectory; panel (b) shows individual rotational components of  
925 the eye. Fig. 14(c) shows out and return trajectories for three other saccade targets; horizontal, vertical and  
926 oblique. The trajectories have characteristic shapes and also show some stochastic variation caused by the  
927 noise in the model [see dashed trajectories in Fig. 14(a)].

928 The return trajectories (magenta lines) showed a distinctly different form from the outward trajectories.  
929 They overshot their destination (the null point) significantly. This resulted from the removal of the TN  
930 activity which was holding the eye at the eccentric target location. Removal of this activity, and thus the  
931 static force exerted by the corresponding extraocular muscle, meant that the eye was subject both to a new  
932 muscular force towards the null point *alongside* the restorative spring force of the lengthened rectus muscle.  
933 This stands as a shortcoming of the model.

### 934 3.5.2 Double steps

935 In another experiment, we probed the response of the model to double step stimuli of the type described  
936 in Becker and Jürgens (1979). In that work, the response of human subjects was investigated when shown  
937 stimuli at  $15^\circ$  and  $30^\circ$  eccentricity with variable delay between the stimuli. If the smaller eccentricity  
938 stimulus was shown first, followed by the more distal on the same side of the field of view, this was called  
939 a ‘staircase’ presentation. We carried out a ‘staircase’ presentation, shown in Fig. 15, where our small  
940 eccentricity luminance was at  $8^\circ$  and our more distal luminance was at  $12^\circ$  (both to the right of centre). **The**  
941 **stimuli could not be presented at  $15^\circ$  and  $30^\circ$  to match the experiment, because  $30^\circ$  saccades were outside**  
942 **the range of the model.**

943 We found that there was a critical time delay between the luminances of about 30 ms. If they were  
944 presented with a delay smaller than this value, then a single, slightly hypermetric saccade was made. This  
945 response type is called a *final angle response*. A delay greater than 30 ms between the stimuli would lead to  
946 double step saccades (a so-called *initial angle response*), with the first saccade arriving at  $8^\circ$  (though with  
947 greater variability than normal), and a second saccade being made to a location hypometric of  $12^\circ$  after a  
948 pause of about 240 ms. Fig. 15(a) shows the mean trajectories from 5 simulations of the staircase doublestep  
949 presentation alongside the result for a single saccade to the final angle of  $12^\circ$ . Dash-dot lines show  $\pm 1$   
950 standard deviation about the mean. The corresponding trajectories are shown in Fig. 15(b).

951 Inspection of the activity maps in FEF and SC\_deep (not shown) indicates that when the  $8^\circ$  target  
952 is illuminated for 30 ms or more, the activity associated with this target angle is able to dominate the  
953 activity, hence the execution of a reasonably accurate saccade. The inhibitory feedback from the SBG then  
954 extinguishes activity in FEF, thalamus and SC, which means that a full 200 ms or more is required to allow  
955 activity in these populations to build up again in order to make the smaller saccade from  $8^\circ$  to  $12^\circ$ . This is  
956 in contrast to experimental findings in which the corrective second saccade is often executed *more quickly*  
957 than if it were programmed on its own (Becker and Jürgens, 1979).

## 4 DISCUSSION

958 The aim of this study was to demonstrate the importance of modelling neurological systems *in concert with*  
959 the biomechanical systems with which they have evolved. We hypothesised that by combining existing  
960 neurophysiological models with an accurate model of a musculo-skeletal system, and then **closing the**  
961 **‘agent-environment-agent’ loop** by allowing the movements of the virtual muscles to modulate sensory

962 feedback to the brain model, shortcomings in the constituent models would be revealed, leading to new  
963 knowledge.

964 To demonstrate the validity of this closed-loop approach, we built an integrated model and then identified  
965 the modifications which were necessary to give it the ability to make accurate movements under one type  
966 of stimulus. We then examined its behaviour with other stimuli. We chose the oculomotor model as a basis  
967 for this study because it has only three degrees of freedom, making it one of the simplest musculo-skeletal  
968 systems. Furthermore, eye movements fall into several well-defined categories, each being controlled by  
969 separate brain circuits, we were therefore justified in modelling a system which produced only saccadic  
970 eye movements. Nevertheless, we are aware that we did not create a complete model of the system; no  
971 treatment of the cerebellum was attempted, justified because cerebellum appears to have only a minor  
972 effect on saccade accuracy (Dean and Porrill, 2008), probably correcting for slow to medium timescale  
973 changes in the physical dynamics of the eyeball (Dean et al., 1994).

974 To summarise our model integration: We combined the Cope-Chambers model (Cope et al., 2017) with a  
975 saccadic burst generator model based on the work of Gancarz and Grossberg (1998), using this to drive the  
976 input of a new biomechanical eye model. To achieve the spatial transformation from the retinotopic maps of  
977 the Cope-Chambers model to the six ‘muscle channel’ inputs for the saccadic burst generator, we used the  
978 mapping of Ottes et al. (1986) to produce parameterised weight maps along with an empirically discovered  
979 synergy for the torsional weight maps. We introduced an additional transformation to the brain model to  
980 achieve invariant sized hills of activity in superior colliculus to fulfil the invariant integral hypothesis of  
981 Tabareau et al. (2007). We closed the loop using a software component which transformed a view of a  
982 world containing luminous cross shapes into the eye’s frame of reference, given its instantaneous rotational  
983 state. This component also computed the inverse of the mapping from Ottes et al. (1986) to project the view  
984 retinotopically into the brain model. This paper serves to describe how we achieved the integration in order  
985 to test our hypothesis, and we intend that the material and methods section, along with the model code  
986 itself, will help others to carry out similar studies. We will discuss what can be learned from an integrated  
987 model of a combined brain and biomechanical system, using our oculomotor system as an example and  
988 then consider how this study compares with other modelling and robotic studies of closed-loop systems.

989 Our integration approach revealed three ways in which this model fails to provide a full understanding  
990 of the saccadic system. In each case, the issue is made clear *as a result of the integration*. This is not to  
991 say that other approaches may not also reveal shortcomings; we will see that one of our cases has been  
992 independently identified (Groh, 2011).

#### 993 4.1 The need for a widening projection field

994 The original combination of the Cope-Chambers model with the theoretical weight maps of Ottes et al.  
995 (1986) and Tabareau et al. (2007) resulted in a model which was able to produce accurate saccades only  
996 along the principle rotational axes (Fig. 10). Thus, *the integration of the models* suggested that an additional  
997 layer was required to achieve accurate saccades for oblique, as well as for horizontal and vertical saccades.  
998 Although the *need* for an invariant integral is discussed in Tabareau et al. (2007) as resulting from their  
999 theoretical study, the mechanism by which such an invariant Gaussian hill is generated is not. By combining  
1000 the models, we were forced to consider this mechanism, and hypothesised that a widening projection field  
1001 would be a candidate mechanism. The results of Fig. 11 indicate that a substantial improvement in accuracy  
1002 is indeed achieved by this new mechanism.

## 1003 4.2 Saccades from non-null starting positions

1004 The implementation of a biophysically accurate model of the eye, and the closed-loop nature of the model  
1005 makes it very natural to consider how the model will behave when making saccades from arbitrary starting  
1006 positions, or how it would respond to a sequence of stimuli. This was the motivation for the out-and-return  
1007 experiment (Fig. 14) as well as for the double step experiment (Fig. 15). We found that return saccades were  
1008 substantially affected by the biomechanics of the eye, as the brain and brainstem model had no mechanism  
1009 to account for the position-dependent restoring forces applied by the eye. This question has been addressed  
1010 by other authors; Groh (2011) investigates the effect of initial eye position on stimulated saccades and finds  
1011 a need for the signal in superior colliculus to be modulated by an eye position signal. Ling et al. (2007)  
1012 shows the existence of a position dependent firing rate offset in abducens neurons. Though we will not  
1013 speculate here on the mechanism by which return saccades may be made accurate whilst also resetting  
1014 the activity of tonic neurons in the SBG, it is interesting that in the model in which we omitted to reset  
1015 TN activity (TModel4), we obtained relatively accurate out-and-return saccades which closely resembled  
1016 experimental data. We suggest that residual activity in TN populations may offer an explanation for how  
1017 the restorative force exerted by the elastic oculomotor muscles is compensated for. A comparison of this  
1018 idea with that of Groh (2011) (that there is a modulation, from a brainstem signal, of the SC readout) would  
1019 make a subject for a future study. Although these existing studies have highlighted this issue, the inaccurate  
1020 return saccades which the model makes from eccentric starting positions provide a clear example of the  
1021 way in which integrating known models into a closed-loop system can highlight deficiencies in the model.

## 1022 4.3 Inhibitory feedback from saccadic burst generator to brain

1023 The third issue raised by the integration of the component models of the saccadic system has, like  
1024 the return saccades, to do with resetting activity. In this case, rather than the reset of activity in the TN  
1025 population in the brainstem, it is the question of how the activity in the *brain* model should be reset after  
1026 each saccade. When a target luminance is projected onto the World population in the model, this induces  
1027 activity which ‘reverberates’ in loops through FEF, basal ganglia, SC and thalamus. The brainstem contains  
1028 a mechanism to limit the timescale of a saccade (inhibitory feedback from EBN, via IBN to LLBN; see  
1029 Fig. 4). However, if the activity in SC is not reset, then following the completion of the first saccade, a  
1030 series of subsequent ‘staircase’ saccades will be executed. There needs to be a mechanism to extinguish  
1031 activity in SC, but also in FEF and thalamus, as activity in either of these populations can build up and  
1032 eventually cause repeat activity in SC and another saccade. We added hypothetical inhibitory feedback  
1033 connections to our model, such that the IBN populations in the SBG would inhibit activity in FEF, thalamus  
1034 and SC\_deep (Fig. 4), preventing the occurrence of staircase saccades.

1035 An examination of the behaviour of the model when presented with ‘double-step stimuli’ reveals a  
1036 problem with our inhibitory feedback connections. We found that when double-step stimuli were presented  
1037 (where an initial target at 8° was replaced with a 12° target after 30 or 40 ms) and a double saccade was  
1038 made [Fig. 15(a), black lines] the second saccade latency was *longer* even than the initial saccade. This  
1039 contrasts with Becker and Jürgens (1979) who find that second, corrective saccades occur with *shorter*  
1040 latencies. This suggests that the inhibitory reset signal implemented in this model is too strong or has the  
1041 wrong timescales. This issue highlights the fact that connections *between* component models are quite as  
1042 important as the connections within each model.

1043 There is some evidence for an inhibitory projection to SC from the brainstem. Corvisier and Hardy  
1044 (1991) offer evidence for a projection from the propositus hypoglossi nucleus. This lies upstream from  
1045 motoneurons and (in primates) encodes eye velocity (Dale and Cullen, 2013), rather than head movement

velocity. Although the propositus hypoglossi does not lie in exactly the same functional location as our IBN population (instead it sits between TN and MN), it offers a possible inhibitory feedback signal proportional to eye velocity and may help to reduce activity in SC post-saccade. Alternatively, it is possible that activity in FEF and thalamus are reset via a ‘timed signal’. Feasibly, after activity in FEF exceeds a threshold, an internal, inhibitory feedback signal could be activated. This inhibition should have a timescale of sufficient duration to reduce activity in FEF, thalamus and, via an increase in inhibitory output from SNr, also in SC. Indeed, the cortical microcircuit contains a variety of morphologically distinct gabaergic neurons (Douglas and Martin, 2004) which could fulfil this functionality. A similar mechanism would then be required in SC, to reset activity generated by direct excitation via the retinal-collicular pathway which generates express saccades. Again, SC is a multi-layered structure, containing gabaergic interneurons (Munoz and Istvan, 1998; Meredith and Ramoa, 1998; Helms et al., 2004; Sooksawate et al., 2011) and there is mounting evidence that saccade dynamics are generated within SC (Kaneda et al., 2008; Goossens and van Opstal, 2012; Bayguinov et al., 2015). Thus, a more complex treatment of the SC and FEF regions in the model may well obviate the need for inhibitory feedback from brainstem to SC, FEF and thalamus.

Considering whether a feedback connection, or internal, recurrent inhibition is responsible for activity-reset in the brain model raises a more general question about modelling the central nervous system. We should consider whether inaccuracies within one part of the model may propagate errors through the closed-loop system that cannot be counteracted by another part of the simulation. There is no way to know, from integrating sub-systems, which properties hold true, and which are false. However, by integrating models and examining the behaviour of the combined model, we are presented with the right questions to ask of the model and the experimental data. In the case of activity-reset, this is to re-assess whether there exists inhibitory feedback from brainstem to the SC and FEF regions, and to find out how an integrated model with self-regulatory mechanisms in SC and FEF may perform.

The omission of the cerebellum will not have escaped the reader’s notice. Whilst many of the nuclei known to be involved in the production of saccadic eye movements are incorporated within the model, the cerebellum is not. The cerebellum is known to play an important rôle in saccade programming (Dean et al., 1994; Schweighofer et al., 1996; Quaia et al., 2000; Kleine, 2003). It may be able to completely replace the functionality of the colliculus when lesioned (Aizawa and Wurtz, 1998; Lefèvre et al., 1998). However, this rôle is typically considered to be one of accuracy tuning (Barash et al., 1999; Dean et al., 1994); operating as an additive model. Furthermore, saccades made by individuals with cerebellar ataxias perform with only moderate loss of saccade accuracy (Barash et al., 1999; Federighi et al., 2011). Because we did not address learning in our model, and because our aim was to demonstrate the utility of integrating brain with biomechanics in order to highlight deficiencies, we considered the omission of the cerebellar nuclei acceptable in the present work.

We have not addressed the question of saccade duration in this paper. Saccade duration is of interest in models which produce two (or three) dimensional saccades, because the dynamics of a saccade follow well known relationships with the saccade eccentricity, regardless of the saccade angle. This causes a problem for models (such as the present one) for which some of the dynamic behaviour is generated within orthogonal components. For example, saccade duration increases with target eccentricity. A 10° eccentricity oblique (45° up and right) saccade is composed (approximately) of a 7° upwards component and a 7° rightwards component. If the component based model is responsible for the dynamics, then the 10° oblique saccade would be expected to have the dynamics of a 7° up or 7° right saccade. This is not found in practice, and the components are said to have been stretched, hence the name for this effect ‘component stretching’. The Gancarz and Grossberg (1998) model is reported to take account of the component stretching effect via

1090 the OPN neuron population. We did not find this effect in our implementation of the model; the duration  
1091 of oblique saccades at a given eccentricity was always substantially different from the duration of the  
1092 corresponding purely vertical or horizontal saccade. Because there is a somewhat complicated interplay  
1093 between the dynamics of the superior colliculus driving the dynamic system of the SBG, we feel this is  
1094 outside the scope of the current work and a subject for a future paper.

#### 1095 4.4 Comparison with other studies

1096 We have called this closed-loop, biomimetic modelling approach *computational neurobehaviour*, in  
1097 which a complete, behaving model is constructed, with attention paid to the biological accuracy of each  
1098 brain and biomechanical sub-system. There already exist many closed-loop *robotic* systems which receive  
1099 sensory input from the world, process that input and generate behaviour by activating motor systems (Yu  
1100 et al., 2004; Fend et al., 2004; Pearson et al., 2007). We now consider whether robotic systems which model  
1101 biological components *in hardware* could fall within our new category. Using a number of examples, we  
1102 will attempt to illustrate what we mean by computational neurobehaviour. We'll consider which examples  
1103 fall into the new category and which are covered by other fields of robotics or computational neuroscience.

1104 Pearson et al. (2007) describes a wheeled robot which has a biomimetic whisker sensory system, along  
1105 with a biomimetic neural system imitating the operation of the rat's sensory processing and controlling  
1106 the movement of the robot. Fend et al. (2004) is a similar, wheeled, whiskered robot, with a repertoire of  
1107 three behaviours organised in a subsumption architecture. In both robots, actions that are selected within  
1108 the brain model drive a non-biologically accurate wheel motor control algorithm to achieve rotational and  
1109 translational movements. Although both have sensory and processing systems which are guided by biology,  
1110 the non-biological motor control stage prevents us from considering these as being studies of computational  
1111 neurobehaviour. Instead, we would refer to these as *embodied models*, as described in Bolado-Gomez and  
1112 Gurney (2013), a study in which the learning behaviour of a biomimetic 'core' model is embedded within  
1113 an engineered 'architecture' (a wheeled robot) which closes the agent-environment loop. Yu et al. (2004)  
1114 report on a biomimetic fish robot, whose motor system closely resembles that of the real fish. The robot  
1115 is able to operate in a closed-loop mode, where sensory input is provided to the non-biomimetic control  
1116 algorithms from overhead cameras, but its control system is also able to operate in open-loop mode. Neither  
1117 the control system, nor the sensory system are biophysically accurate and we would not describe this study  
1118 as computational neurobehaviour. Nevertheless, the biophysically accurate motor system they describe has  
1119 the potential to form part of a computational neurobehavioural study of swimming behaviour in the fish, if  
1120 it were combined in a loop with suitable sensory input and sensory processing models. Knips et al. (2017)  
1121 is a report of a reach-and-grasp robot arm controlled via a dynamic neural field brain model. The sensory  
1122 input for this system—its 'eyes'—is a Microsoft Kinect sensor; it also has somatosensory feedback from  
1123 the fingers of the robot's hand. The neural field 'brain' controls the seven degrees of freedom of the arm to  
1124 carry out the reach-and-grasp action. While this robot has closed-loop control and is clearly inspired by  
1125 biology, it remains a study of robotics and of the improvement of the control of the robot's reach-and-grasp  
1126 function, rather than a study which aims to learn more about the biology of a primate arm. For this reason,  
1127 we would describe the study of Knips et al. (2017) as an embodied model.

1128 To summarise, in most closed-loop robotic studies which incorporate neuro-mimetic models, the hardware  
1129 forms an 'engineered surround architecture', allowing for the examination of the behaviour of the embodied  
1130 model. However, suitably *biomimetic* hardware such as the fish in Yu et al. (2004) would not be excluded  
1131 from computational neurobehavioural studies.

1132 Modern programming platforms, often originating from the computer game industry, make it relatively  
1133 easy to model a virtual environment. Consequently, an increasing number of studies into robotic or neuro-  
1134 mimetic control are carried out with virtual robots operating within a virtual environment. N'Guyen et al.  
1135 (2014) and Thurat et al. (2015) are two studies of the oculomotor system which model sensory input, neural  
1136 control *and* motor output in software. These studies fall outside the remit of computational neurobehaviour  
1137 only because they omit to close the sensory loop. DeWolf et al. (2016) describes a reach model comprising  
1138 a simplified virtual arm (with fewer degrees of freedom than a primate arm), and a biologically inspired  
1139 brain model. This model also omits to close the sensory feedback loop and we consider it a computational  
1140 neuroscience study of a (virtually) embodied model.

1141 There are also experimental closed-loop approaches to understanding sensorimotor control. Ejaz et al.  
1142 (2013) places a fly in a fixed position, and couples it with a free-to-move robot. The sensory input collected  
1143 by the robot is projected onto the eyes of the fly, and activity from a selected neuron in the fly's brain  
1144 is used to drive a control system for the robot's movements. This allows the experimenters to study the  
1145 behaviour of the fly's brain operating in a closed-loop condition that is more natural than the open-loop  
1146 condition that many other experimental techniques mandate. The results from closed-loop experiments will  
1147 undoubtedly inform future neurobehavioural models.

1148 Thus, while there are many models that close the agent-environment loop and display partial biological  
1149 plausibility, the biomimetic features are usually confined to a sub-system of the entire model. This leads us  
1150 to formalise a definition of computational neurobehaviour as: *The study of biological sensory-motor system*  
1151 *behaviour using biologically accurate models of sensory input, brain and motor sub-systems operating in*  
1152 *a closed-loop*. We believe our oculomotor model is one of the first such models using this approach and  
1153 shares many features with that of Arena et al. (2017) which describes a robotic insect system based on  
1154 the fly species *Drosophila Melanogaster*. It has biomimetic insect legs implemented in a virtual robot and  
1155 a neuro-mimetic brain. Closing the loop is a visual sensory input system which is able to determine the  
1156 distance between the robot and an obstacle and the obstacle's height. The authors demonstrate that the  
1157 virtual robot is able to learn to climb obstacles in a realistic manner and suggest that the model may be  
1158 compared with experimental data from future *Drosophila* experiments addressing obstacle climbing and  
1159 learning. The visual system is not described in detail, but if it is modelled in a biologically plausible manner,  
1160 then this work may reasonably be described as a computational neurobehaviour study, contemporaneous  
1161 with our own.

## DISCLOSURE/CONFLICT-OF-INTEREST STATEMENT

1162 The authors declare that the research was conducted in the absence of any commercial or financial  
1163 relationships that could be construed as a potential conflict of interest.

## AUTHOR CONTRIBUTIONS

1164 SJ, AB and AC implemented existing parts of the model in SpineML. AB developed the saccade generator  
1165 brainstem model. SJ performed the technical and scientific integration of the biomechanical eye. CP and  
1166 KM developed the biomechanical eye model. SJ wrote the manuscript; SA, AB, KG and KM contributed  
1167 to the manuscript. KG conceived the project.

## ACKNOWLEDGEMENTS

1168 Funding: European Union FP7 Grant 610391 ‘NoTremor’.

## SUPPLEMENTAL DATA

1169 The model specification, results and all code required to reproduce the results of this work are available at:  
1170 [https://github.com/ABRG-Models/OMM\\_NeuroMuscular](https://github.com/ABRG-Models/OMM_NeuroMuscular)

## REFERENCES

- 1171 Aizawa, H. and Wurtz, R. H. (1998). Reversible inactivation of monkey superior colliculus. I. Curvature of  
1172 saccadic trajectory. *Journal of neurophysiology* 79, 2082–2096
- 1173 Alex Cope and Paul Richmond (2014). SpineML. RRID: SCR\_015641
- 1174 Anderson, R. W., Keller, E. L., Gandhi, N. J., and Das, S. (1998). Two-dimensional saccade-related  
1175 population activity in superior colliculus in monkey. *Journal of Neurophysiology* 80, 798–817
- 1176 Arai, K., Keller, E., and Edelman, J. (1994). Two-dimensional neural network model of the primate  
1177 saccadic system. *Neural Networks* 7, 1115. doi:10.1016/S0893-6080(05)80162-5
- 1178 Arai, K. and Keller, E. L. (2005). A model of the saccade-generating system that accounts for trajectory  
1179 variations produced by competing visual stimuli. *Biological cybernetics* 92, 21–37. doi:10.1007/  
1180 s00422-004-0526-y
- 1181 Arena, E., Arena, P., Strauss, R., and Patané, L. (2017). Motor-Skill Learning in an Insect Inspired  
1182 Neuro-Computational Control System. *Frontiers in Neurorobotics* 11. doi:10.3389/fnbot.2017.00012
- 1183 Bahill, A. T. and Stark, L. (1979). The trajectories of saccadic eye movements. *Scientific American* 240,  
1184 108–117
- 1185 Barash, S., Melikyan, A., Sivakov, A., Zhang, M., Glickstein, M., and Thier, P. (1999). Saccadic dysmetria  
1186 and adaptation after lesions of the cerebellar cortex. *Journal of Neuroscience* 19, 10931–10939
- 1187 Bayguinov, P. O., Ghitani, N., Jackson, M. B., and Basso, M. A. (2015). A Hard-Wired Priority Map  
1188 in the Superior Colliculus Shaped by Asymmetric Inhibitory Circuitry. *Journal of Neurophysiology*  
1189 doi:10.1152/jn.00144.2015
- 1190 Becker, W. and Jürgens, R. (1979). An analysis of the saccadic system by means of double step stimuli.  
1191 *Vision Research* 19, 967–983. doi:10.1016/0042-6989(79)90222-0
- 1192 Bevan, M. D. and Wilson, C. J. (1999). Mechanisms underlying spontaneous oscillation and rhythmic  
1193 firing in rat subthalamic neurons. *The Journal of neuroscience : the official journal of the Society for  
1194 Neuroscience* 19, 7617–28
- 1195 Blenkinsop, A., Anderson, S., and Gurney, K. (2017). Frequency and function in the basal ganglia: the  
1196 origins of beta and gamma band activity. *The Journal of Physiology* doi:10.1113/JP273760
- 1197 Bogacz, R. and Gurney, K. (2007). The basal ganglia and cortex implement optimal decision making  
1198 between alternative actions. *Neural Computation* 19, 442–477. doi:10.1162/neco.2007.19.2.442
- 1199 Bolado-Gomez, R. and Gurney, K. (2013). A biologically plausible embodied model of action discovery.  
1200 *Frontiers in Neurorobotics* 7. doi:10.3389/fnbot.2013.00004
- 1201 Bolam, J., Hanley, J., Booth, P., and Bevan, M. (2000). Synaptic organisation of the basal ganglia. *Journal  
1202 of Anatomy* 196, 527–542
- 1203 Brown, P., Oliviero, A., Mazzone, P., Insola, A., Tonali, P., and Di Lazzaro, V. (2001). Dopamine  
1204 Dependency of Oscillations between Subthalamic Nucleus and Pallidum in Parkinson’s Disease. *J.  
1205 Neurosci.* 21, 1033–1038

- 1206 Bruce, C. J. and Goldberg, M. E. (1985). Primate frontal eye fields. I. Single neurons discharging before  
1207 saccades. *Journal of Neurophysiology* 53, 603–635
- 1208 Casteau, S. and Vitu, F. (2012). On the effect of remote and proximal distractors on saccadic behavior: A  
1209 challenge to neural-field models. *Journal of vision* 12, 14
- 1210 Chambers, J. M., Gurney, K., Humphries, M., and Prescott, A. (2012). Mechanisms of choice in the  
1211 primate brain: a quick look at positive feedback. In *Modelling Natural Action Selection* (Cambridge  
1212 University Press). 390–420
- 1213 Chen, L. L. and Wise, S. P. (1995). Supplementary eye field contrasted with the frontal eye field during  
1214 acquisition of conditional oculomotor associations. *Journal of Neurophysiology* 73, 1122–1134
- 1215 Chevalier, G. and Deniau, J. M. (1990). Disinhibition as a basic process in the expression of striatal  
1216 functions. *Trends in Neurosciences* 13, 277–280
- 1217 Cohen, J. Y., Heitz, R. P., Woodman, G. F., and Schall, J. D. (2009). Neural basis of the set-size effect in  
1218 frontal eye field: timing of attention during visual search. *Journal of Neurophysiology* 101, 1699–1704.  
1219 doi:10.1152/jn.00035.2009
- 1220 Cope, A., Chambers, J. M., Prescott, T. J., and Gurney, K. N. (2017). Basal Ganglia Control Of  
1221 Reflexive Saccades: A Computational Model Integrating Physiology Anatomy And Behaviour. *bioRxiv*  
1222 doi:10.1101/135251
- 1223 Cope, A. and Gurney, K. N. (2011). A biologically based model of active vision. In *Proceedings of  
1224 AISB'11 - Architectures for Active Vision*, eds. S. O'Keefe, Kazakov, D., and Tsoulas, D. (York, UK),  
1225 13–20
- 1226 Cope, A. J. and James, S. S. (2015). SpineML\_2\_brahms (NoTremor Oculomotor branch)
- 1227 Cope, A. J., Richmond, P., and Allerton, D. (2014). The SpineML toolchain: enabling computational neu-  
1228 roscience through flexible tools for creating, sharing, and simulating neural models. *BMC Neuroscience*  
1229 15, P224
- 1230 Cope, A. J., Richmond, P., and James, S. S. (2015). SpineCreator. RRID: SCR\_015637
- 1231 Cope, A. J., Richmond, P., James, S. S., Gurney, K., and Allerton, D. J. (2016). SpineCreator: a  
1232 Graphical User Interface for the Creation of Layered Neural Models. *Neuroinformatics* doi:10.1007/  
1233 s12021-016-9311-z
- 1234 Corvisier, J. and Hardy, O. (1991). Possible excitatory and inhibitory feedback to the superior colliculus: a  
1235 combined retrograde and immunocytochemical study in the prepositus hypoglossi nucleus of the guinea  
1236 pig. *Neuroscience Research* 12, 486–502. doi:10.1016/S0168-0102(09)80002-3
- 1237 Dale, A. and Cullen, K. E. (2013). The nucleus prepositus predominantly outputs eye movement-  
1238 related information during passive and active self-motion. *Journal of Neurophysiology* 109, 1900.  
1239 doi:10.1152/jn.00788.2012
- 1240 Daniel, P. M. and Whitteridge, D. (1961). The representation of the visual field on the cerebral cortex in  
1241 monkeys. *The Journal of Physiology* 159, 203–221. doi:10.1113/jphysiol.1961.sp006803
- 1242 Dean, P. (1995). Modelling the role of the cerebellar fastigial nuclei in producing accurate saccades: the  
1243 importance of burst timing. *Neuroscience* 68, 1059–1077
- 1244 Dean, P., Mayhew, J. E., and Langdon, P. (1994). Learning and maintaining saccadic accuracy: a model of  
1245 brainstemcerebellar interactions. *Journal of Cognitive Neuroscience* 6, 117–138
- 1246 Dean, P. and Porrill, J. (2008). Adaptive filter models of the cerebellum: computational analysis. *Cerebellum*  
1247 7, 567–571
- 1248 Delgado, A., Sierra, A., Querejeta, E., Valdiosera, R., and Aceves, J. (1999). Inhibitory control of the  
1249 GABAergic transmission in the rat neostriatum by D2 dopamine receptors. *Neuroscience* 95, 1043–1048.  
1250 doi:10.1016/S0306-4522(99)00495-9

- 1251 DeLong, M., Crutcher, M. D., and Georgopoulos, A. (1985). Primate globus pallidus and subthalamic  
1252 nucleus: functional organization. *Journal of Neurophysiology* 53, 530–543
- 1253 Deubel, H. and Schneider, W. X. (1996). Saccade target selection and object recognition: Evidence for a  
1254 common attentional mechanism. *Vision Research* 36, 1827–1837. doi:10.1016/0042-6989(95)00294-4
- 1255 DeWolf, T., Stewart, T. C., Slotine, J.-J., and Eliasmith, C. (2016). A spiking neural model of adaptive arm  
1256 control. *Proceedings of the Royal Society B: Biological Sciences* 283, 20162134. doi:10.1098/rspb.2016.  
1257 2134
- 1258 Dorris, M. C., Paré, M., and Munoz, D. P. (1997). Neuronal Activity in Monkey Superior Colliculus  
1259 Related to the Initiation of Saccadic Eye Movements. *The Journal of Neuroscience* 17, 8566
- 1260 Douglas, R. J. and Martin, K. A. C. (2004). Neuronal Circuits of the Neocortex. *Annual Review of  
1261 Neuroscience* 27, 419–451. doi:10.1146/annurev.neuro.27.070203.144152
- 1262 Edelman, J. A. and Keller, E. L. (1996). Activity of visuomotor burst neurons in the superior colliculus  
1263 accompanying express saccades. *Journal of Neurophysiology* 76, 908
- 1264 Ejaz, N., Krapp, H. G., and Tanaka, R. J. (2013). Closed-loop response properties of a visual interneuron  
1265 involved in fly optomotor control. *Frontiers in Neural Circuits* 7. doi:10.3389/fncir.2013.00050
- 1266 Federighi, P., Cevenini, G., Dotti, M. T., Rosini, F., Pretegiani, E., Federico, A., et al. (2011). Differences  
1267 in saccade dynamics between spinocerebellar atrophy 2 and late-onset cerebellar ataxias. *Brain* 134,  
1268 879–891. doi:10.1093/brain/awr009
- 1269 Fend, M., Bovet, S., and Hafner, V. (2004). The artificial mouse—a robot with whiskers and vision.  
1270 *Proceedings of the 35th International Symposium on Robotics, Paris, 2004.*, 1–6
- 1271 Fuchs, A. and Luschei, E. (1970). Firing patterns of abducens neurons of alert monkeys in relationship to  
1272 horizontal eye movement. *Journal of Neurophysiology* 33, 382–392
- 1273 Funahashi, S., Chafee, M. V., and Goldman-Rakic, P. S. (1993). Prefrontal neuronal activity in rhesus  
1274 monkeys performing a delayed anti-saccade task. *Nature* 365, 753
- 1275 Galvan, A. and Wichmann, T. (2008). Pathophysiology of Parkinsonism. *Clinical Neurophysiology* 119,  
1276 1459–1474. doi:10.1016/j.clinph.2008.03.017
- 1277 Gancarz, G. and Grossberg, S. (1998). A neural model of the saccade generator in the reticular formation.  
1278 *Neural Networks* 11, 1159–1174. doi:10.1016/S0893-6080(98)00096-3
- 1279 Gaymard, B., Ploner, C. J., Rivaud, S., Vermersch, A. I., and Pierrot-Deseilligny, C. (1998). Cortical  
1280 control of saccades. *Experimental Brain Research* 123, 159–163. doi:10.1007/s002210050557
- 1281 Gerfen, C. R., Engbar, T. M., Mahan, L. C., Susel, Z., Chase, T. N., Monsma, F. J., et al. (1990). D1 and  
1282 D2 dopamine receptor regulated gene-expression of striatonigral and striatopallidal neurons. *Science*  
1283 250, 1429–1432
- 1284 Ghitani, N., Bayguinov, P. O., Vokoun, C. R., McMahon, S., Jackson, M. B., and Basso, M. A. (2014).  
1285 Excitatory Synaptic Feedback from the Motor Layer to the Sensory Layers of the Superior Colliculus.  
1286 *The Journal of Neuroscience* 34, 6822–6833. doi:10.1523/JNEUROSCI.3137-13.2014
- 1287 Gian G. Mascetti and Jorge R. Arriagada (1981). Tectotectal interactions through the commissure of the  
1288 superior colliculi. An electrophysiological study. *Experimental Neurology* 71, 122–133
- 1289 Girard, B. and Berthoz, A. (2005). From brainstem to cortex: Computational models of saccade generation  
1290 circuitry. *Progress in Neurobiology* 77, 215–251. doi:10.1016/j.pneurobio.2005.11.001
- 1291 Goldberg, M. E. and Wurtz, R. H. (1972). Activity of superior colliculus in behaving monkey. I. Visual  
1292 receptive fields of single neurons. *J Neurophysiol* 35, 542–559
- 1293 Gonon, F. (1997). Prolonged and extrasynaptic excitatory action of dopamine mediated by D1 receptors in  
1294 the rat striatum in vivo. *The Journal of neuroscience : the official journal of the Society for Neuroscience*  
1295 17, 5972–8

- 1296 Goossens, H. (2006). Dynamic Ensemble Coding of Saccades in the Monkey Superior Colliculus. *Journal*  
1297 *of Neurophysiology* 95, 2326–2341. doi:10.1152/jn.00889.2005
- 1298 Goossens, H. and van Opstal, A. J. (2012). Optimal control of saccades by spatial-temporal activity patterns  
1299 in the monkey superior colliculus. *PLoS computational biology* 8, e1002508
- 1300 Grantyn, A., Brandi, A.-M., Dubayle, D., Graf, W., Ugolini, G., Hadjidimitrakis, K., et al. (2002).  
1301 Density gradients of trans-synaptically labeled collicular neurons after injections of rabies virus in the  
1302 lateral rectus muscle of the rhesus monkey. *The Journal of Comparative Neurology* 451, 346–361.  
1303 doi:10.1002/cne.10353
- 1304 Groh, J. M. (2001). Converting neural signals from place codes to rate codes. *Biological cybernetics* 85,  
1305 159–165
- 1306 Groh, J. M. (2011). Effects of Initial Eye Position on Saccades Evoked by Microstimulation in the Primate  
1307 Superior Colliculus: Implications for Models of the SC Read-Out Process. *Frontiers in Integrative*  
1308 *Neuroscience* 4. doi:10.3389/fnint.2010.00130
- 1309 Gurney, K., Prescott, T. J., and Redgrave, P. (2001a). A computational model of action selection in the  
1310 basal ganglia. I. A new functional anatomy. *Biological cybernetics* 84, 401–10
- 1311 Gurney, K., Prescott, T. J., and Redgrave, P. (2001b). A computational model of action selection in the  
1312 basal ganglia. II. Analysis and simulation of behaviour. *Biological cybernetics* 84, 411–23
- 1313 Hallworth, N. E., Wilson, C. J., and Bevan, M. D. (2003). Apamin-sensitive small conductance calcium-  
1314 activated potassium channels, through their selective coupling to voltage-gated calcium channels, are  
1315 critical determinants of the precision, pace, and pattern of action potential generation in rat subthalamic  
1316 nucleus neurons in vitro. *The Journal of neuroscience* 23, 7525–7542
- 1317 Harsing, L. G. and Zigmond, M. J. (1997). Influence of dopamine on GABA release in striatum: evidence  
1318 for D1-D2 interactions and non-synaptic influences. *Neuroscience* 77, 419–29
- 1319 Hazy, T. E., Frank, M. J., and O'Reilly, R. C. (2007). Towards an executive without a homunculus:  
1320 computational models of the prefrontal cortex/basal ganglia system. *Philosophical Transactions of the*  
1321 *Royal Society B: Biological Sciences* 362, 1601–1613. doi:10.1098/rstb.2007.2055
- 1322 Helms, M. C., Özen, G., and Hall, W. C. (2004). Organization of the Intermediate Gray Layer of the  
1323 Superior Colliculus. I. Intrinsic Vertical Connections. *Journal of Neurophysiology* 91, 1706–1715.  
1324 doi:10.1152/jn.00705.2003
- 1325 Hepp, K. and Henn, V. (1983). Spatio-temporal recoding of rapid eye movement signals in the monkey  
1326 paramedian pontine reticular formation (PPRF). *Experimental brain research* 52, 105–120
- 1327 Hepp, K., Van Opstal, A. J., Straumann, D., Hess, B. J., and Henn, V. (1993). Monkey superior colliculus  
1328 represents rapid eye movements in a two-dimensional motor map. *Journal of neurophysiology* 69,  
1329 965–979
- 1330 Hernández-López, S., Bargas, J., Surmeier, D. J., Reyes, A., and Galarraga, E. (1997). D1 receptor  
1331 activation enhances evoked discharge in neostriatal medium spiny neurons by modulating an L-type  
1332 Ca<sup>2+</sup> conductance. *The Journal of neuroscience : the official journal of the Society for Neuroscience* 17,  
1333 3334–42
- 1334 Herrero, L., Corvisier, J., Hardy and, O., and Torres, B. (1998). Influence of the tectal zone on the  
1335 distribution of synaptic boutons in the brainstem of goldfish. *The Journal of Comparative Neurology*  
1336 401, 411–428. doi:10.1002/(SICI)1096-9861(19981123)401:3<411::AID-CNE8>3.0.CO;2-2
- 1337 Hikosaka, O., Takikawa, Y., and Kawagoe, R. (2000). Role of the basal ganglia in the control of purposive  
1338 saccadic eye movements. *Physiological reviews* 80, 953–978

- 1339 Hikosaka, O. and Wurtz, R. H. (1983). Visual and oculomotor functions of monkey substantia nigra  
1340 pars reticulata. IV. Relation of substantia nigra to superior colliculus. *Journal of neurophysiology* 49,  
1341 1285–301
- 1342 Howard, L. A. and Tipper, S. (1997). Hand deviations away from visual cues: indirect evidence for  
1343 inhibition. *Experimental brain research* 113, 144–152
- 1344 Humphries, M. D. and Gurney, K. N. (2002). The role of intra-thalamic and thalamocortical circuits in  
1345 action selection. *Network: Computation in Neural Systems* 13, 131–156
- 1346 INCF Task Force on Multi-Scale Modeling (2011). Network Interchange for Neuroscience Modeling  
1347 Language (NineML)
- 1348 Isa, T. (2002). Intrinsic processing in the mammalian superior colliculus. *Current Opinion in Neurobiology*  
1349 12, 668–677. doi:10.1016/S0959-4388(02)00387-2
- 1350 Isa, T. and Hall, W. C. (2009). Exploring the Superior Colliculus In Vitro. *Journal of Neurophysiology*  
1351 102, 2581–2593. doi:10.1152/jn.00498.2009
- 1352 James, S., Bell, O. A., Nazli, M. A. M., Pearce, R. E., Spencer, J., Tyrrell, K., et al. (2017). Target-distractor  
1353 synchrony affects performance in a novel motor task for studying action selection. *PLOS ONE* 12,  
1354 e0176945. doi:10.1371/journal.pone.0176945
- 1355 Jayaraman, A., Batton, R. R., and Carpenter, M. B. (1977). Nigrotectal projections in the monkey: an  
1356 autoradiographic study. *Brain research* 135, 147–152
- 1357 Jiang, H., Stein, B. E., and McHaffie, J. G. (2003). Opposing basal ganglia processes shape midbrain  
1358 visuomotor activity bilaterally. *Nature* 423, 982–986. doi:10.1038/nature01698
- 1359 Kaneda, K., Phongphanphanee, P., Katoh, T., Isa, K., Yanagawa, Y., Obata, K., et al. (2008). Regulation of  
1360 Burst Activity through Presynaptic and Postsynaptic GABAB Receptors in Mouse Superior Colliculus.  
1361 *Journal of Neuroscience* 28, 816–827. doi:10.1523/JNEUROSCI.4666-07.2008
- 1362 Kita, H. and Kitai, S. T. (1991). Intracellular study of rat globus pallidus neurons: membrane properties  
1363 and responses to neostriatal, subthalamic and nigral stimulation. *Brain research* 564, 296–305
- 1364 Kleine, J. F. (2003). Saccade-Related Neurons in the Primate Fastigial Nucleus: What Do They Encode?  
1365 *Journal of Neurophysiology* 90, 3137–3154. doi:10.1152/jn.00021.2003
- 1366 Knips, G., Zibner, S. K. U., Reimann, H., and Schöner, G. (2017). A Neural Dynamic Architecture for  
1367 Reaching and Grasping Integrates Perception and Movement Generation and Enables On-Line Updating.  
1368 *Frontiers in Neurorobotics* 11. doi:10.3389/fnbot.2017.00009
- 1369 Kühn, A. A., Williams, D., Kupsch, A., Limousin, P., Hariz, M., Schneider, G.-H., et al. (2004). Event-  
1370 related beta desynchronization in human subthalamic nucleus correlates with motor performance. *Brain*  
1371 : a journal of neurology 127, 735–46. doi:10.1093/brain/awh106
- 1372 Latto, R. (1977). The effects of bilateral frontal eye-field, posterior parietal or superior collicular lesions  
1373 on brightness thresholds in the rhesus monkey. *Neuropsychologia* 15, 507–516
- 1374 Lee, C., Rohrer, W. H., and Sparks, D. L. (1988). Population coding of saccadic eye movements by neurons  
1375 in the superior colliculus. *Nature* 332, 357–360. doi:10.1038/332357a0
- 1376 Lefèvre, P., Quaia, C., and Optican, L. M. (1998). Distributed model of control of saccades by superior  
1377 colliculus and cerebellum. *Neural Networks* 11, 1175–1190
- 1378 Linden, R. and Perry, V. (1983). Massive retinotectal projection in rats. *Brain research* 272, 145–149
- 1379 Ling, L., Fuchs, A. F., Siebold, C., and Dean, P. (2007). Effects of initial eye position on saccade-related  
1380 behavior of abducens nucleus neurons in the primate. *Journal of Neurophysiology* 98, 3581–3599
- 1381 Lynch, J. C., Hoover, J. E., and Strick, P. L. (1994). Input to the primate frontal eye field from the substantia  
1382 nigra, superior colliculus, and dentate nucleus demonstrated by transneuronal transport. *Experimental*  
1383 *Brain Research* 100, 181–186

- 1384 Maes, P. (1989). *The dynamics of action selection* (Artificial Intelligence Laboratory, Vrije Universiteit  
1385 Brussel)
- 1386 Marcos, E. and Genovesio, A. (2016). Determining Monkey Free Choice Long before the Choice Is Made:  
1387 The Principal Role of Prefrontal Neurons Involved in Both Decision and Motor Processes. *Frontiers in  
1388 Neural Circuits* 10. doi:10.3389/fncir.2016.00075
- 1389 Marino, R. A., Trappenberg, T. P., Dorris, M., and Munoz, D. P. (2012). Spatial Interactions in the Superior  
1390 Colliculus Predict Saccade Behavior in a Neural Field Model. *Journal of Cognitive Neuroscience* 24,  
1391 315–336. doi:10.1162/jocn\_a\_00139
- 1392 Massone, L. L. E. (1994). A neural-network system for control of eye movements: basic mechanisms.  
1393 *Biological Cybernetics* 71, 293–305. doi:10.1007/BF00239617
- 1394 Mays, L. E. and Sparks, D. L. (1980). Dissociation of visual and saccade-related responses in superior  
1395 colliculus neurons. *Journal of Neurophysiology* 43, 207–232
- 1396 McCarthy, M. M., Moore-Kochlacs, C., Gu, X., Boyden, E. S., Han, X., and Kopell, N. (2011). Striatal  
1397 origin of the pathologic beta oscillations in Parkinson's disease. *Proceedings of the National Academy  
1398 of Sciences* 108, 11620–11625. doi:10.1073/pnas.1107748108
- 1399 McFarland, N. R. and Haber, S. N. (2002). Thalamic relay nuclei of the basal ganglia form both reciprocal  
1400 and nonreciprocal cortical connections, linking multiple frontal cortical areas. *Journal of Neuroscience*  
1401 22, 8117–8132
- 1402 McIlwain, J. T. (1982). Lateral spread of neural excitation during microstimulation in intermediate gray  
1403 layer of cat's superior colliculus. *Journal of Neurophysiology* 47, 167–178
- 1404 McPeek, R. M. (2006). Incomplete Suppression of Distractor-Related Activity in the Frontal Eye Field  
1405 Results in Curved Saccades. *Journal of Neurophysiology* 96, 2699–2711. doi:10.1152/jn.00564.2006
- 1406 McPeek, R. M., Han, J. H., and Keller, E. L. (2003). Competition Between Saccade Goals in the Superior  
1407 Colliculus Produces Saccade Curvature. *Journal of Neurophysiology* 89, 2577–2590. doi:10.1152/jn.  
1408 00657.2002
- 1409 McPeek, R. M. and Keller, E. L. (2002). Saccade Target Selection in the Superior Colliculus During a  
1410 Visual Search Task. *Journal of Neurophysiology* 88, 2019–2034
- 1411 Meredith, M. A. and Ramoa, A. S. (1998). Intrinsic Circuitry of the Superior Colliculus: Pharmacophysiological  
1412 Identification of Horizontally Oriented Inhibitory Interneurons. *Journal of Neurophysiology* 79,  
1413 1597–1602
- 1414 Middleton, F. A. and Strick, P. L. (2000). Basal ganglia and cerebellar loops: motor and cognitive circuits.  
1415 *Brain Research Reviews* 31, 236–250. doi:10.1016/S0165-0173(99)00040-5
- 1416 Mink, J. (1996). The basal ganglia: Focused selection and inhibition of competing motor programs.  
1417 *Progress in Neurobiology* 50, 381–425
- 1418 Mink, J. W. and Thach, W. T. (1993). Basal ganglia intrinsic circuits and their role in behavior. *Current  
1419 opinion in Neurobiology* 3, 950–957
- 1420 Mitchinson, B., Chan, T.-S., Chambers, J., Pearson, M., Humphries, M., Fox, C., et al. (2010). BRAHMS:  
1421 Novel middleware for integrated systems computation. *Advanced Engineering Informatics* 24, 49–61.  
1422 doi:10.1016/j.aei.2009.08.002
- 1423 Mitchinson, B. and James, S. S. (2015). BRAHMS. RRID: SCR\_015642
- 1424 Monosov, I. E., Trageser, J. C., and Thompson, K. G. (2008). Measurements of simultaneously recorded  
1425 spiking activity and local field potentials suggest that spatial selection emerges in the frontal eye field.  
1426 *Neuron* 57, 614–625

- 1427 Morén, J., Shibata, T., and Doya, K. (2013). The Mechanism of Saccade Motor Pattern Generation  
1428 Investigated by a Large-Scale Spiking Neuron Model of the Superior Colliculus. *PLoS ONE* 8, e57134.  
1429 doi:10.1371/journal.pone.0057134
- 1430 Moschovakis, A. K., Kitama, T., Dalezios, Y., Petit, J., Brandi, A. M., and Grantyn, A. A. (1998). An  
1431 Anatomical Substrate for the Spatiotemporal Transformation. *Journal of Neuroscience* 18, 10219–10229
- 1432 Munoz, D. P. (2002). Commentary: Saccadic eye movements: overview of neural circuitry. In *Progress in*  
1433 *Brain Research*, ed. D. M. J. Hyona, W. Heide and R. Radach (Elsevier), vol. Volume 140. 89–96
- 1434 Munoz, D. P. and Everling, S. (2004). Look away: the anti-saccade task and the voluntary control of eye  
1435 movement. *Nature Reviews Neuroscience* 5, 218–228. doi:10.1038/nrn1345
- 1436 Munoz, D. P. and Istvan, P. J. (1998). Lateral inhibitory interactions in the intermediate layers of the  
1437 monkey superior colliculus. *Journal of Neurophysiology* 79, 1193–1209
- 1438 Nambu, A., Yoshida, S.-i., and Jinnai, K. (1990). Discharge patterns of pallidal neurons with input from  
1439 various cortical areas during movement in the monkey. *Brain Research* 519, 183–191. doi:10.1016/  
1440 0006-8993(90)90076-N
- 1441 N'Guyen, S., Thurat, C., and Girard, B. (2014). Saccade learning with concurrent cortical and subcortical  
1442 basal ganglia loops. *Frontiers in Computational Neuroscience* 8. doi:10.3389/fncom.2014.00048
- 1443 Norman, D. A. and Shallice, T. (1986). Attention to action. In *Consciousness and self-regulation* (Springer).  
1444 1–18
- 1445 Nowotny, T. (2011). Flexible neuronal network simulation framework using code generation for NVidia®  
1446 CUDA™. *BMC Neuroscience* 12, P239. doi:10.1186/1471-2202-12-S1-P239
- 1447 Nowotny, T., Cope, A. J., Yavuz, E., Stimberg, M., Goodman, D. F., Marshall, J., et al. (2014). SpineML  
1448 and Brian 2.0 interfaces for using GPU enhanced Neuronal Networks (GeNN). *BMC Neuroscience* 15,  
1449 P148. doi:10.1186/1471-2202-15-S1-P148
- 1450 Olivier, E., Corvisier, J., Pauluis, Q., and Hardy, O. (2000). Evidence for glutamatergic tectotectal neurons  
1451 in the cat superior colliculus: a comparison with GABAergic tectotectal neurons. *European Journal of*  
1452 *Neuroscience* 12, 2354–2366
- 1453 Ottes, F. P., Van Gisbergen, J. A., and Eggermont, J. J. (1986). Visuomotor fields of the superior colliculus:  
1454 A quantitative model. *Vision Research* 26, 857–873. doi:10.1016/0042-6989(86)90144-6
- 1455 Papapavlou, C. and Moustakas, K. (2014). Physics-based modelling and animation of saccadic eye  
1456 movement
- 1457 Parent, A. and Hazrati, L. (1993). Anatomical aspects of information processing in primate basal ganglia.  
1458 *Trends in Neuroscience* 16, 111–116
- 1459 Pearson, M. J., Pipe, A. G., Melhuish, C., Hutchinson, B., and Prescott, T. J. (2007). Whiskerbot: A robotic  
1460 active touch system modeled on the rat whisker sensory system. *Adaptive Behaviour* 15
- 1461 Quaia, C., Lefèvre, P., and Optican, L. M. (1999). Model of the Control of Saccades by Superior Colliculus  
1462 and Cerebellum. *Journal of Neurophysiology* 82, 999
- 1463 Quaia, C., Paré, M., Wurtz, R. H., and Optican, L. M. (2000). Extent of compensation for variations  
1464 in monkey saccadic eye movements. *Experimental Brain Research* 132, 39–51. doi:10.1007/  
1465 s002219900324
- 1466 Redgrave, P., Prescott, T. J., and Gurney, K. (1999). The basal ganglia: a vertebrate solution to the selection  
1467 problem? *Neuroscience* 89, 1009–1023
- 1468 Reppert, T. R., Lempert, K. M., Glimcher, P. W., and Shadmehr, R. (2015). Modulation of Saccade  
1469 Vigor during Value-Based Decision Making. *Journal of Neuroscience* 35, 15369–15378. doi:10.1523/  
1470 JNEUROSCI.2621-15.2015

- 1471 Reulen, J. P. H. (1984). Latency of visually evoked saccadic eye movements. *Biological Cybernetics* 50,  
1472 251–262. doi:10.1007/BF00337075
- 1473 Richmond, P. (2015). DAMSON
- 1474 Richmond, P., Cope, A., Gurney, K., and Allerton, D. J. (2014). From Model Specification to Simulation  
1475 of Biologically Constrained Networks of Spiking Neurons. *Neuroinformatics* 12, 307–323. doi:10.1007/  
1476 s12021-013-9208-z
- 1477 Robinson, D. (1972). Eye movements evoked by collicular stimulation in the alert monkey. *Vision Research*  
1478 12, 1795–1808. doi:10.1016/0042-6989(72)90070-3
- 1479 Robinson, D. A. (1975). Oculomotor control signals. In *Basic mechanisms of ocular motility and their  
1480 clinical implications*, eds. G. Lennerstrand and P. Bach-y Rita (Oxford: Pergamon). 337–374
- 1481 Robinson, D. A. and Fuchs, A. F. (1969). Eye movements evoked by stimulation of frontal eye fields.  
1482 *Journal of Neurophysiology* 32, 637–648
- 1483 Rovamo, J. and Virsu, V. (1979). An estimation and application of the human cortical magnification factor.  
1484 *Experimental Brain Research* 37, 495–510. doi:10.1007/BF00236819
- 1485 Sabes, P. N., Breznen, B., and Andersen, R. A. (2002). Parietal representation of object-based saccades.  
1486 *Journal of Neurophysiology* 88, 1815–1829
- 1487 Saint-Cyr, J. A., Ungerleider, L. G., and Desimone, R. (1990). Organization of visual cortical inputs to the  
1488 striatum and subsequent outputs to the pallidonigral complex in the monkey. *Journal of Comparative  
1489 Neurology* 298, 129–156
- 1490 Schall, J. D., Hanes, D. P., Thompson, K. G., and King, D. J. (1995). Saccade target selection in frontal  
1491 eye field of macaque .1. Visual and premovement activation. *Journal of Neuroscience* 15, 6905–6918
- 1492 Schall, J. D. and Thompson, K. G. (1999). Neural selection and control of visually guided eye movements.  
1493 *Annual review of neuroscience* 22, 241–259
- 1494 Schiller, P. H., Sandell, J. H., and Maunsell, J. H. (1987). The effect of frontal eye field and superior  
1495 colliculus lesions on saccadic latencies in the rhesus monkey. *Journal of Neurophysiology* 57, 1033
- 1496 Schlag, J. D. (2002). Neurons that program what to do and in what order. *Neuron* 34, 177–178
- 1497 Schwartz, E. L. (1977). Spatial mapping in the primate sensory projection: Analytic structure and relevance  
1498 to perception. *Biological Cybernetics* 25, 181–194. doi:10.1007/BF01885636
- 1499 Schwartz, E. L. (1980). Computational anatomy and functional architecture of striate cortex: A spatial  
1500 mapping approach to perceptual coding. *Vision Res.* 20, 645–669
- 1501 Schweighofer, N., Arbib, M. A., and Dominey, P. F. (1996). A model of the cerebellum in adaptive control  
1502 of saccadic gain. *Biological Cybernetics* 75, 19–28
- 1503 Scudder, C. A. (1988). A new local feedback model of the saccadic burst generator. *J Neurophysiol* 59,  
1504 1454
- 1505 Segraves, M. A. and Goldberg, M. E. (1987). Functional properties of corticotectal neurons in the monkey's  
1506 frontal eye field. *Journal of Neurophysiology* 58, 1387–1419
- 1507 Seth, A., Sherman, M., Reinbolt, J. a., and Delp, S. L. (2011). OpenSim: a musculoskeletal modeling  
1508 and simulation framework for in silico investigations and exchange. *Procedia IUTAM* 2, 212–232.  
1509 doi:10.1016/j.piutam.2011.04.021
- 1510 Slotnick, S. D., Klein, S. A., Carney, T., and Sutter, E. E. (2001). Electrophysiological estimate of human  
1511 cortical magnification. *Clinical Neurophysiology* 112, 1349–1356
- 1512 Sommer, M. A. and Wurtz, R. H. (2000). Composition and topographic organization of signals sent from  
1513 the frontal eye field to the superior colliculus. *Journal of Neurophysiology* 83, 1979–2001

- 1514 Sooksawate, T., Isa, K., Behan, M., Yanagawa, Y., and Isa, T. (2011). Organization of GABAergic  
1515 inhibition in the motor output layer of the superior colliculus. *European Journal of Neuroscience* 33,  
1516 421–432. doi:10.1111/j.1460-9568.2010.07535.x
- 1517 Sparks, D. L. (2002). The brainstem control of saccadic eye movements. *Nature Reviews Neuroscience* 3,  
1518 952–964. doi:10.1038/nrn986
- 1519 Sparks, D. L. and Nelson, I. S. (1987). Sensory and motor maps in the mammalian superior colliculus.  
1520 *Trends in Neurosciences* 10, 312–317. doi:10.1016/0166-2236(87)90085-3
- 1521 Stanton, G. B., Goldberg, M. E., and Bruce, C. J. (1988a). Frontal eye field efferents in the macaque  
1522 monkey: I. Subcortical pathways and topography of striatal and thalamic terminal fields. *Journal of  
1523 Comparative Neurology* 271, 473–492. doi:10.1002/cne.902710402
- 1524 Stanton, G. B., Goldberg, M. E., and Bruce, C. J. (1988b). Frontal eye field efferents in the macaque  
1525 monkey: II. Topography of terminal fields in midbrain and pons. *The Journal of Comparative Neurology*  
1526 271, 493–506. doi:10.1002/cne.902710403
- 1527 Sterling, P. (1971). Receptive fields and synaptic organization of the superficial gray layer of the cat  
1528 superior colliculus. *Vision Research* 11, 309–IN47. doi:10.1016/0042-6989(71)90048-4
- 1529 Tabareau, N., Bennequin, D., Berthoz, A., Slotine, J.-J., and Girard, B. (2007). Geometry of the superior  
1530 colliculus mapping and efficient oculomotor computation. *Biological cybernetics* 97, 279–292
- 1531 Takagi, M., Zee, D. S., and Tamargo, R. J. (1998). Effects of Lesions of the Oculomotor Vermis on Eye  
1532 Movements in Primate: Saccades. *Journal of Neurophysiology* 80, 1911
- 1533 Talbot, S. and Marshall, W. (1941). Physiological Studies on Neural Mechanisms of Visual Localization  
1534 and Discrimination\*. *American Journal of Ophthalmology* 24, 1255–1264. doi:10.1016/S0002-9394(41)  
1535 91363-6
- 1536 Tehovnik, E. J., Sommer, M. A., Chou, I.-H., Slocum, W. M., and Schiller, P. H. (2000). Eye fields in the  
1537 frontal lobes of primates. *Brain Research Reviews* 32, 413–448. doi:10.1016/S0165-0173(99)00092-2
- 1538 Thelen, D. G. (2003). Adjustment of Muscle Mechanics Model Parameters to Simulate Dynamic  
1539 Contractions in Older Adults. *Journal of Biomechanical Engineering* 125, 70. doi:10.1115/1.1531112
- 1540 Thivierge, J.-P. and Marcus, G. F. (2007). The topographic brain: from neural connectivity to cognition.  
1541 *Trends in Neurosciences* 30, 251–259. doi:10.1016/j.tins.2007.04.004
- 1542 Thompson, K. G. and Bichot, N. P. (2005). A visual salience map in the primate frontal eye field. In  
1543 *Progress in Brain Research*, eds. J. van Pelt, M. Kamermans, C. N. Levelt, A. van Ooyen, G. J. A.  
1544 Ramakers, and P. R. Roelfsema (Elsevier), vol. 147 of *Development, Dynamics and Pathology of  
1545 Neuronal Networks: from Molecules to Functional Circuits*. 249–262
- 1546 Thompson, K. G., Bichot, N. P., and Sato, T. R. (2005). Frontal eye field activity before visual search errors  
1547 reveals the integration of bottom-up and top-down salience. *Journal of Neurophysiology* 93, 337–351
- 1548 Thurat, C., NGuyen, S., and Girard, B. (2015). Biomimetic race model of the loop between the superior  
1549 colliculus and the basal ganglia: Subcortical selection of saccade targets. *Neural Networks* 67, 54–73.  
1550 doi:10.1016/j.neunet.2015.02.004
- 1551 Tipper, S. P., Howard, L. A., and Paul, M. A. (2001). Reaching affects saccade trajectories. *Experimental  
1552 Brain Research* 136, 241–249
- 1553 Ungerleider, L. G. and Mishkin, M. (1982). Two cortical visual systems. In *Analysis of Visual Behavior*,  
1554 eds. D. J. Ingle, A. M. Goodale, and R. J. W. Mansfield (Cambridge, MA: MIT Press). 549–586
- 1555 Van Gisbergen, J., Van Opstal, A., and Tax, A. (1987). Collicular ensemble coding of saccades based on  
1556 vector summation. *Neuroscience* 21, 541–555. doi:10.1016/0306-4522(87)90140-0
- 1557 Van Gisbergen, J. A. M., Van Opstal, A. J., and Schoenmakers, J. J. M. (1985). Experimental test of two  
1558 models for the generation of oblique saccades. *Experimental brain research* 57, 321–336

- 1559 van Opstal, A. J. and Goossens, H. H. L. M. (2008). Linear ensemble-coding in midbrain superior colliculus  
1560 specifies the saccade kinematics. *Biological Cybernetics* 98, 561–577. doi:10.1007/s00422-008-0219-z
- 1561 Van Opstal, A. J., Hepp, K., Hess, B. J., Straumann, D., and Henn, V. (1991). Two-rather than three-  
1562 dimensional representation of saccades in monkey superior colliculus. *Science* 252, 1313–1315
- 1563 van Opstal, A. J. and van Gisbergen, J. A. (1990). Role of monkey superior colliculus in saccade averaging.  
1564 *Experimental Brain Research* 79, 143–149
- 1565 Vokoun, C. R., Huang, X., Jackson, M. B., and Basso, M. A. (2014). Response Normalization in the  
1566 Superficial Layers of the Superior Colliculus as a Possible Mechanism for Saccadic Averaging. *Journal*  
1567 *of Neuroscience* 34, 7976–7987. doi:10.1523/JNEUROSCI.3022-13.2014
- 1568 Vokoun, C. R., Jackson, M. B., and Basso, M. A. (2010). Intralaminar and Interlaminar Activity within the  
1569 Rodent Superior Colliculus Visualized with Voltage Imaging. *Journal of Neuroscience* 30, 10667–10682.  
1570 doi:10.1523/JNEUROSCI.1387-10.2010
- 1571 Vokoun, C. R., Jackson, M. B., and Basso, M. A. (2011). Circuit dynamics of the superior colliculus  
1572 revealed by in vitro voltage imaging: Vokoun et al. *Annals of the New York Academy of Sciences* 1233,  
1573 41–47. doi:10.1111/j.1749-6632.2011.06166.x
- 1574 Waitzman, D. M., Ma, T. P., Optican, L. M., and Wurtz, R. H. (1991). Superior colliculus neurons mediate  
1575 the dynamic characteristics of saccades. *Journal of Neurophysiology* 66, 1716–1737
- 1576 Walker, R., Deubel, H., Schneider, W. X., and Findlay, J. M. (1997). Effect of remote distractors on saccade  
1577 programming: evidence for an extended fixation zone. *Journal of neurophysiology* 78, 1108–1119
- 1578 Wickens, J. (1997). Basal ganglia: structure and computations. *Network: Computation in Neural Systems*  
1579 8, 77–109
- 1580 Wilson, C. and Kawaguchi, Y. (1996). The origins of the two-state spontaneous membrane potential  
1581 fluctuations of neostriatal spiny neurons. *The Journal of Neuroscience* 16, 2397–2410
- 1582 Wilson, C. J. (2004). A Model of Reverse Spike Frequency Adaptation and Repetitive Firing of Subthalamic  
1583 Nucleus Neurons. *Journal of Neurophysiology* 91, 1963–1980. doi:10.1152/jn.00924.2003
- 1584 Wu, H. H., Williams, C. V., and McLoon, S. C. (1994). Involvement of nitric oxide in the elimination  
1585 of a transient retinotectal projection in development. *SCIENCE-NEW YORK THEN WASHINGTON-*,  
1586 1593–1593
- 1587 Wurtz, R. H. and Albano, J. E. (1980). Visual-motor function of the primate superior colliculus. *Annual*  
1588 *review of Neuroscience* 3, 189–226. doi:10.1146/annurev.ne.03.030180.001201
- 1589 Wurtz, R. H. and Goldberg, M. E. (1972). Activity of superior colliculus in behaving monkey. III. Cells  
1590 discharging before eye movements. *J Neurophysiol* 35, 575–586
- 1591 Yu, J., Tan, M., Wang, S., and Chen, E. (2004). Development of a biomimetic robotic fish and its control  
1592 algorithm. *IEEE Transactions on System, Man and Cybernetics - Part B* 34, 1798–1810

## FIGURES

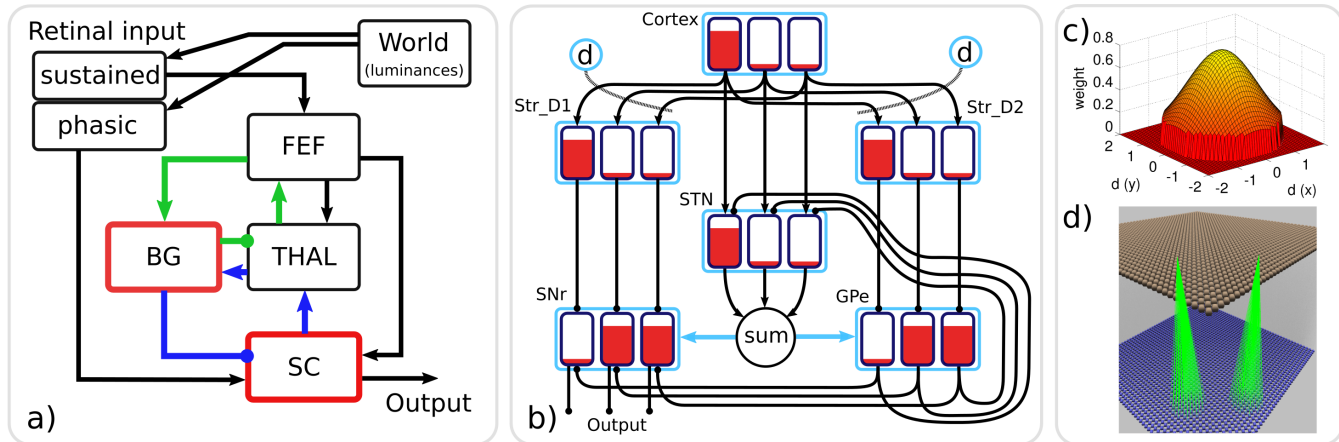


**Figure 1. a) The macroscopic architecture of the Cope-Chambers model.** The main nuclei modelled as brain systems are: basal ganglia (BG), frontal eye fields (FEF), thalamus (THAL) and superior colliculus (SC). The retinal input is presented via non-biologically plausible retinal populations. The loops through basal ganglia, which define the architecture, are shown with coloured lines: the cortical loop (through FEF and THAL) in green and the sub-cortical loop (through SC and THAL) in blue. Connections with arrowheads indicate excitatory connections, those with circles are inhibitory. A red border indicates that the box represents a sub-system of two or more populations; a black box indicates (at least, within the context of the model) a single neural population. The BG box is expanded in: **b) The basal ganglia model component.** This shows a basal ganglia comprising striatum (Str\_D1 & Str\_D2), substantia nigra reticulata (SNr). The model has three action channels shown as black boxes within each blue population border. Three channels of cortical input to the BG are also depicted. Red indicates the activation level of a given channel, helping to illustrate the selection mechanism. For example, the channel indicated by the leftmost bar has a high salience (cortical input) and excites activity in Str\_D1 which then inhibits the leftmost bar in SNr. The diffuse projection from STN is equivalent to summing its projections channel-wise, and then projecting the sum to all channels of its target populations (the blue arrows indicate that all channels of GPe and SNr are targeted by the connection). Dopaminergic modulation of the inputs to the striatum are indicated by the blue circles labelled 'd' and the dotted lines. The SNr sends inhibitory output projections to its targets. **c) 2D Gaussian weights.** The 'GaussianKernel' connectivity pattern is based on the 'in-plane displacement' between the location of a neural element in one layer, and the location of a target neural element in the target layer for the connection. The potential weight of the connection is given by a 2D Gaussian function, which is maximum for the target neuron which exactly corresponds to the source neuron, and drops down for target neurons which are horizontally displaced from the source neuron. A threshold is applied to avoid a computationally expensive all-to-all connectivity (with most of these connections having negligible weight values). If the weight is non-zero, then a connection is made from source to target, otherwise no connection is made. **d) Gaussian connectivity.** This image shows connectivity (green rays) from two source neurons (in Str\_D2, brown spheres) to target neurons (in GPe, blue spheres). The circular connectivity pattern is seen. This does not show the weight values, which reduce 'towards the edge of the circle' and follow the relationship shown in (c).

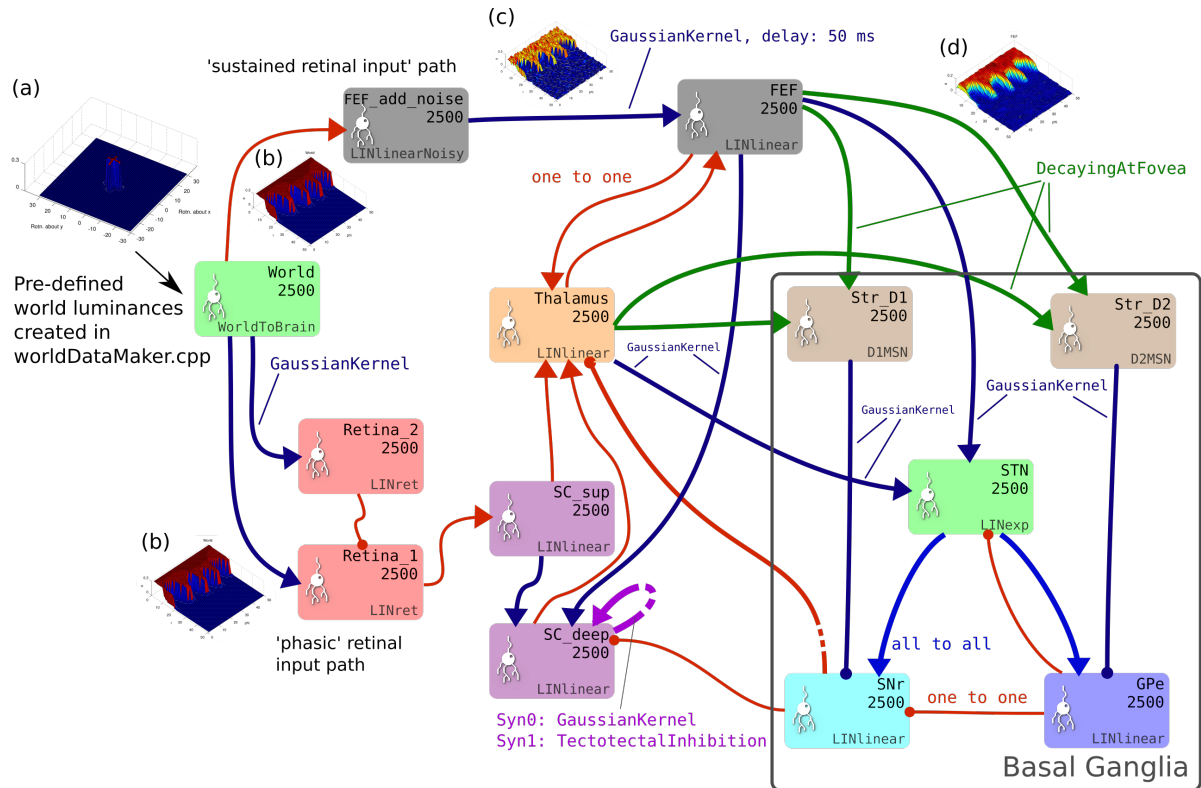


**Figure 2.** The brain model. This is the SpineCreator ‘network layer’ view of the model. Each box represents a neural population with 2500 elements, arranged in a  $50 \times 50$  grid. The SpineML component name is printed on the bottom right corner of each population box and the population name is at the top. The overall connectivity between populations is represented by the projection arrows with the colour indicating the connectivity scheme (one-to-one connections are red, Gaussian kernel connections are dark blue and so on). Excitatory connections have arrowheads and inhibitory connections have circles, although for details of the behaviour of the connections, the weight-update and post-synapse components must be studied. Briefly, the model comprises a *World* population, into which a retinotopically organised view of the world is introduced. This information is passed into cortical populations (FEF) and subcortical populations (SC) via a simple model of the retina. These feed a cortico-thalamo-basal ganglia loop, which selects which region of the deep layer of superior colliculus should be disinhibited, allowing activity to build up therein. The five populations comprising the basal ganglia are enclosed in a grey outline. Note that substantia nigra pars compacta is not modelled here, instead the level of dopamine in the striatum is set via a parameter in the Str.D1 and Str.D2 populations

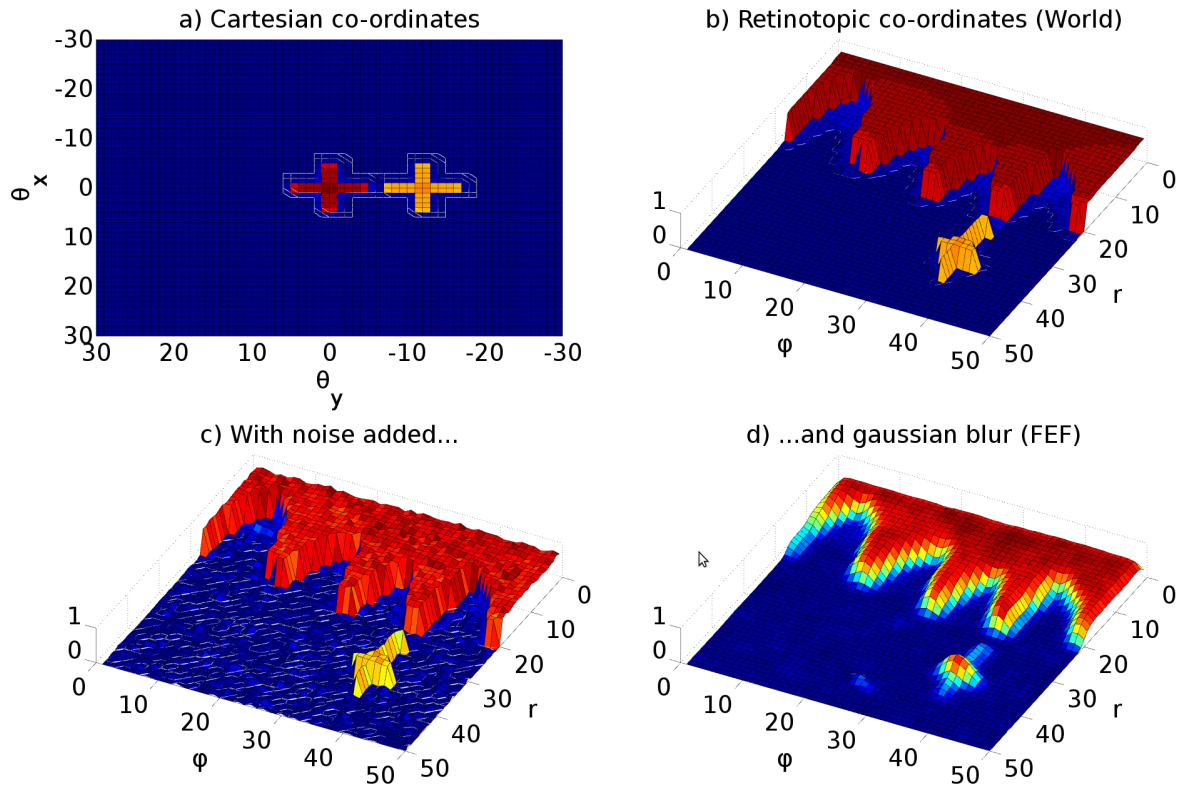


**Figure 3.** Representative mapping from eye's frame of reference in Cartesian co-ordinates to retinotopic co-ordinates. (a) The mapping of luminances in the eye's frame of reference. The world input is pre-defined by a JSON configuration file. Luminance position, size and shape can be defined in this file, along with the times at which luminances appear and disappear. The `worldDataMaker.cpp` code computes the locations of the luminances in the eye's frame of reference, given its rotational state. It also computes a 2D Gaussian convolution of the luminances. Here, there are two cross shaped luminances spanning  $10^\circ$ , one of value 0.8 at the fixation point (0,0) and one of value 0.5 at a peripheral position (0,-12°). Note that these crosses have the same 'bar width' of  $2^\circ$  as the crosses used in the simulations, but their span of  $10^\circ$  is greater than the  $6^\circ$  used in the simulations, to make these images clearer. (b) The locations of the luminances in the eye's frame of reference are then converted into retinotopic co-ordinates, with centrally located luminances being represented at low values of  $r$  and more peripheral luminances having higher values of  $r$ .  $\phi$  encodes rotational angle: 1 and 50 encode upward movement; 13 is left; 25 is down; 37 is right. The output of the World component is fed into `FEF_add_noise` and into the retinal neuron populations. The colour map makes it possible to distinguish between the two crosses. (c) The `FEF_add_noise` populations adds a level of noise to the signal representing processing of the signal in visual cortex. (d) A Gaussian projection from `FEF_add_noise` to `FEF` further blurs the activity in `FEF`. `FEF` is the input to the basal ganglia and one input to superior colliculus.

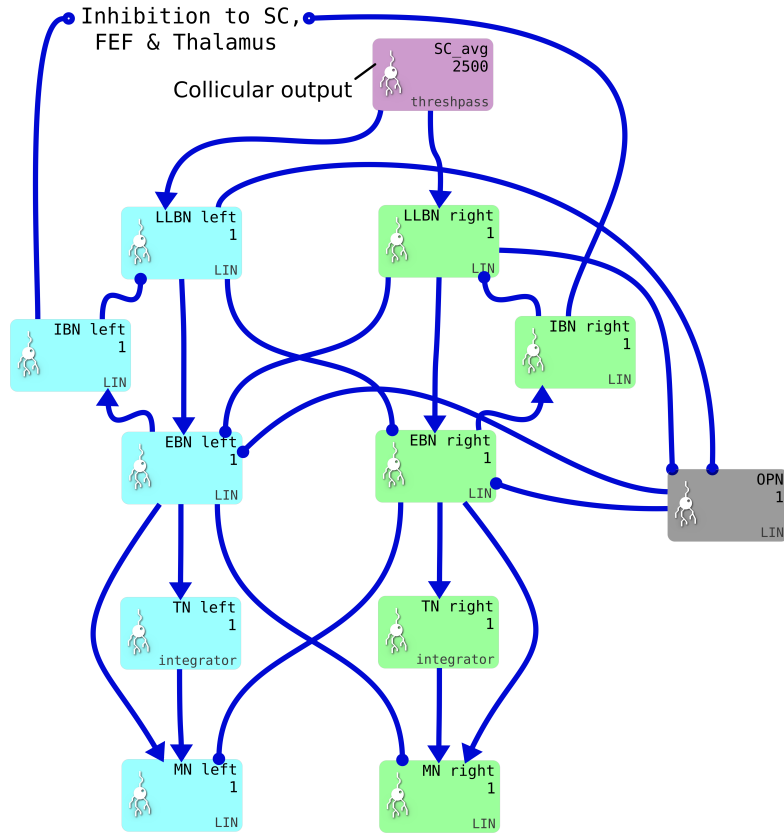


**Figure 4.** One pair of channels of the saccadic burst generator (SBG) for left (cyan) or right (green) movements. Collicular activity in SC\_avg excites the channels via SBG weight maps. Each box represents a neural population and shows the population name, the number of neural elements (here 2500 or 1) and the SpineML component name; LIN for Leaky integrator or *integrator*. Key: LLBN: Long lead burst neurons; IBN: Inhibitory burst neurons; OPN: Omnipause neurons; EBN: Excitatory burst neurons; TN: Tonic neurons; MN: Motoneurons.

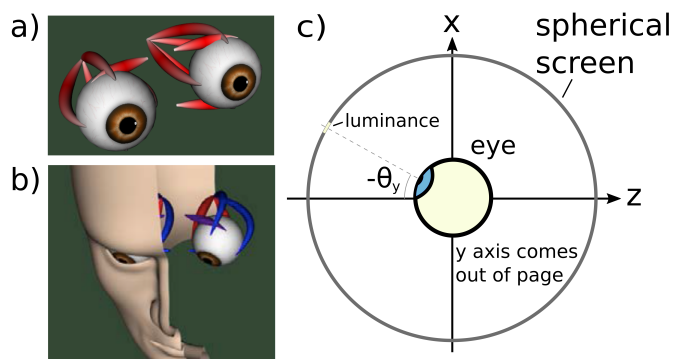


**Figure 5.** The biomechanical eye. a) an OpenSim rendering of a pair of biomechanical eyes showing the positions of the extraocular muscles. Note that i) volume visualization of muscles should not be confused with FEM muscle models; it is provided for user feedback purposes, i.e. shape and color change depending on the muscle activation, ii) superior and inferior oblique are visualized up to their respective muscle pulleys. b) OpenSim rendering of biomechanical eye within a head model c) Top-down schematic cross-sectional view of the biomechanical eye situated within a spherical screen, with a horizontal rotation towards a luminance at an angle of  $-\theta_y$  about the  $y$  axis. The  $y$  axis points up, out of the page.

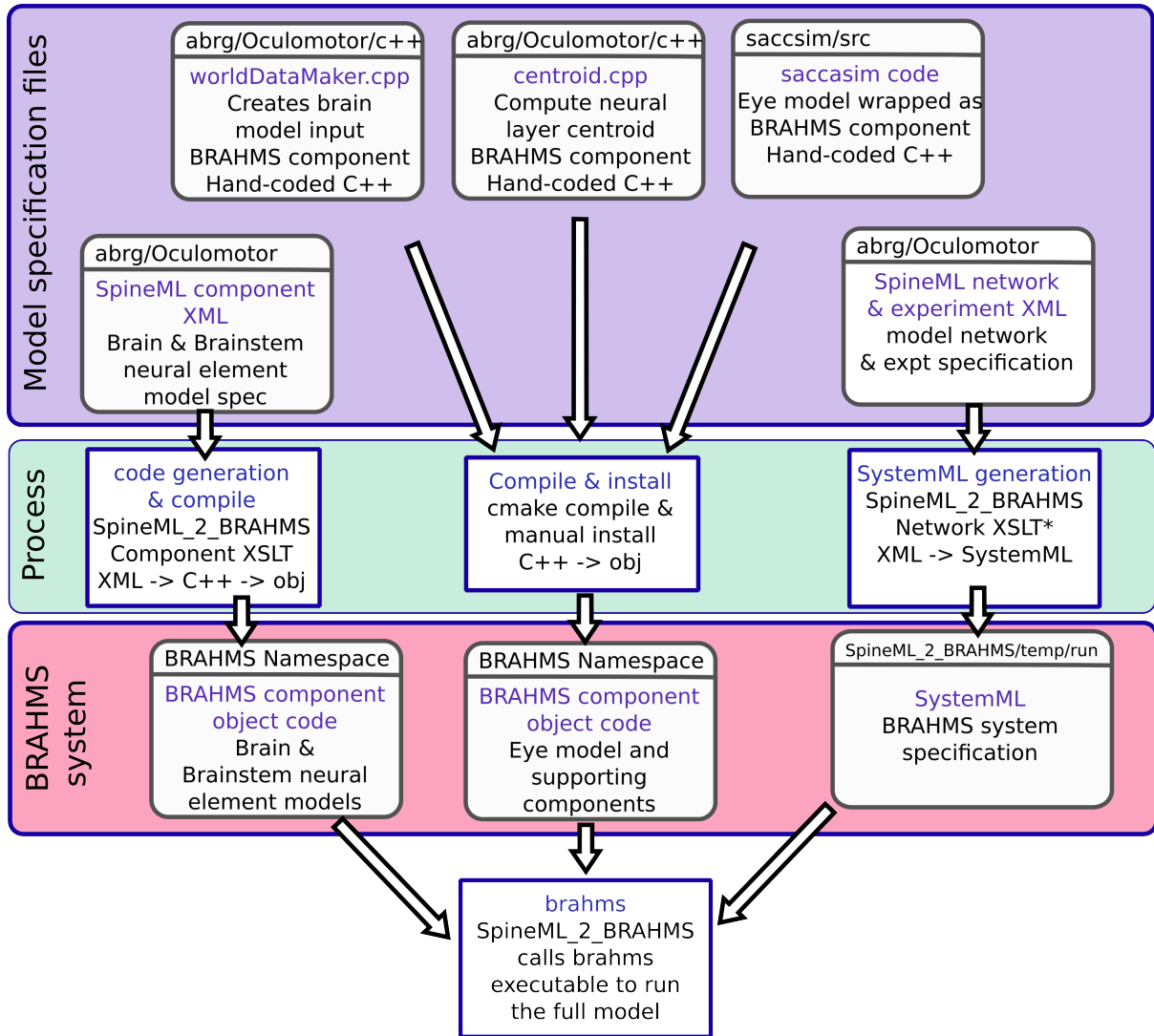


**Figure 6.** The model framework. The model is specified using a combination of declarative XML files and hand-coded C++. These original model specifications are shown within the blue box. b) The green box shows the processes which are applied to the model specification to produce the BRAHMS system. Most of the process is defined within the scripts which make up SpineML\_2\_BRAHMS, but the hand-written components must be manually compiled and installed within the BRAHMS Namespace, allowing the BRAHMS executable to locate them at runtime. c) The red box shows the resulting BRAHMS system ready to be executed by the BRAHMS executable. In practice, this call is made by SpineML\_2\_BRAHMS.

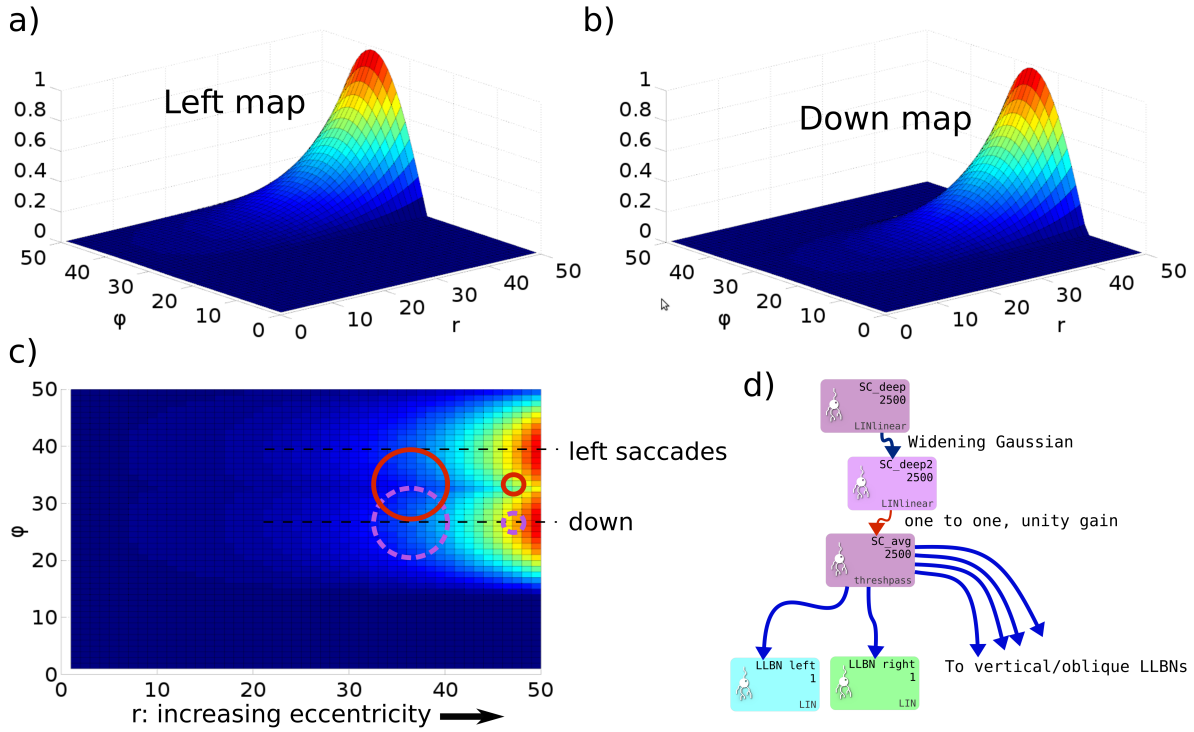


**Figure 7.** a) & b) Tabareau-style weight maps for ‘left’ and ‘down’ components of a saccade. c) The two weight maps in a) and b) shown on the same graph, viewed from above. Circles show the locations of potential hills of activity. Purple, dashed circles encode saccades down; red circles encode saccades with both a left and a down component. d) Showing the additional deep layer of superior colliculus (SC\_deep2) and the output layer (SC\_avg, named for the fact that in an earlier version of the model, it received the output of the centroid of SC\_deep). The widening Gaussian projection is shown as the arrow between SC\_deep and SC\_deep2.

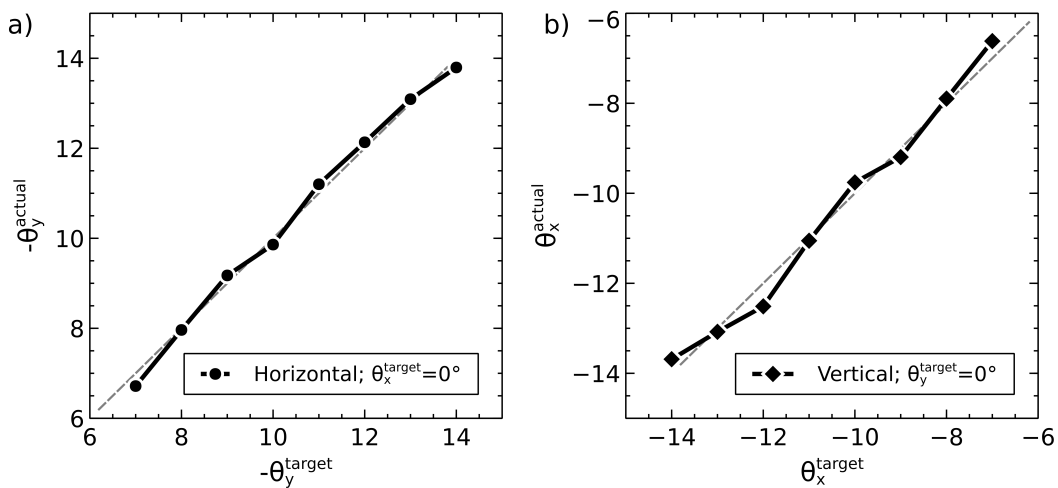


**Figure 8.** Accuracy at different target eccentricities for fixation luminance 0.2 and target luminance 0.3.

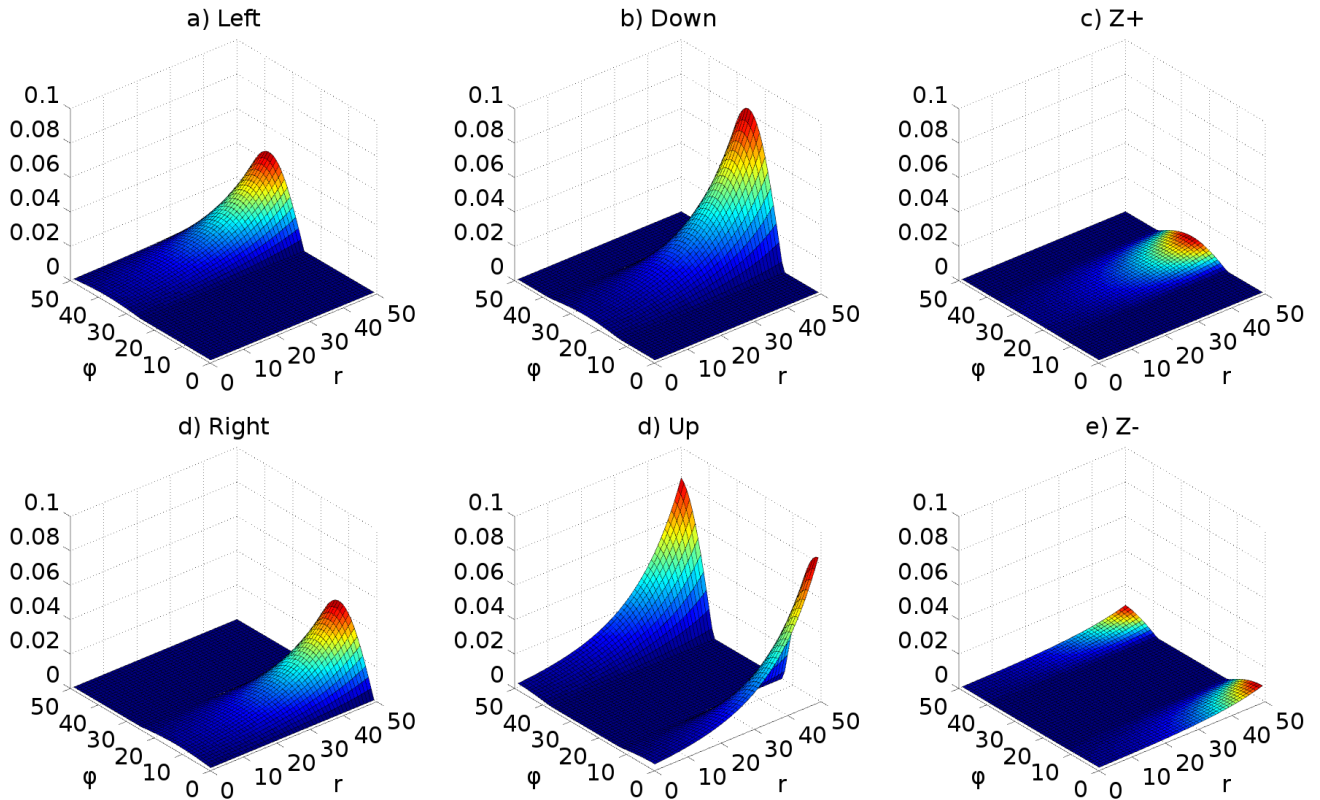


**Figure 9.** Weight maps for the connections between the output layer of superior colliculus and the six long lead burst neurons of the saccadic burst generator model. Each map increases exponentially with increasing  $r$ , multiplied by  $\cos(\phi)$  about its ‘active’ axis.

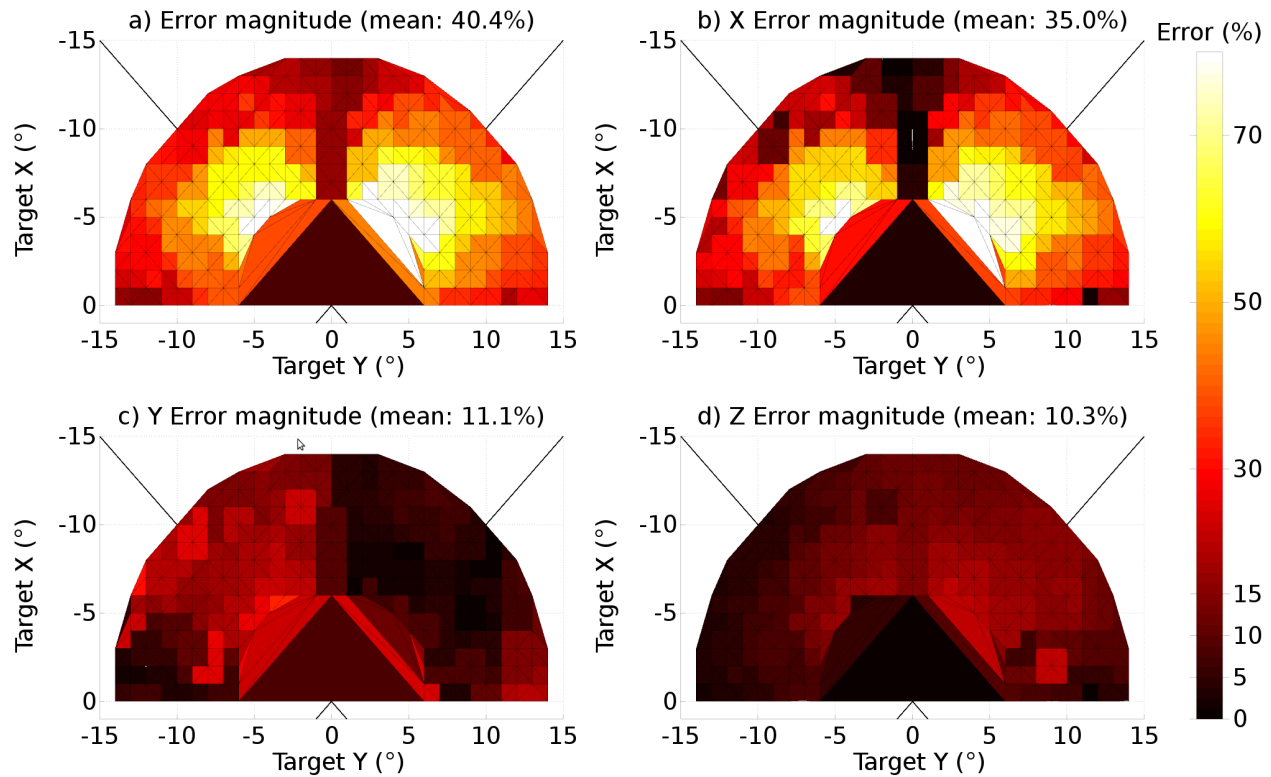


**Figure 10.** The end-point error surface for the original, naïve model (TModel3). a) The ratio of the magnitudes of the total error vector and the target vector, expressed as a percentage. b) The ratio of the magnitude of the  $x$  component of the error vector to the magnitude of the target vector, expressed as a percentage. c) As (b) but for the  $y$  component. d) As (b), for  $z$  component. All colour maps are shown with the same scale. The target rotations,  $\theta_x^t$  and  $\theta_y^t$  are denoted ‘Target X’ and ‘Target Y’ in the figure.

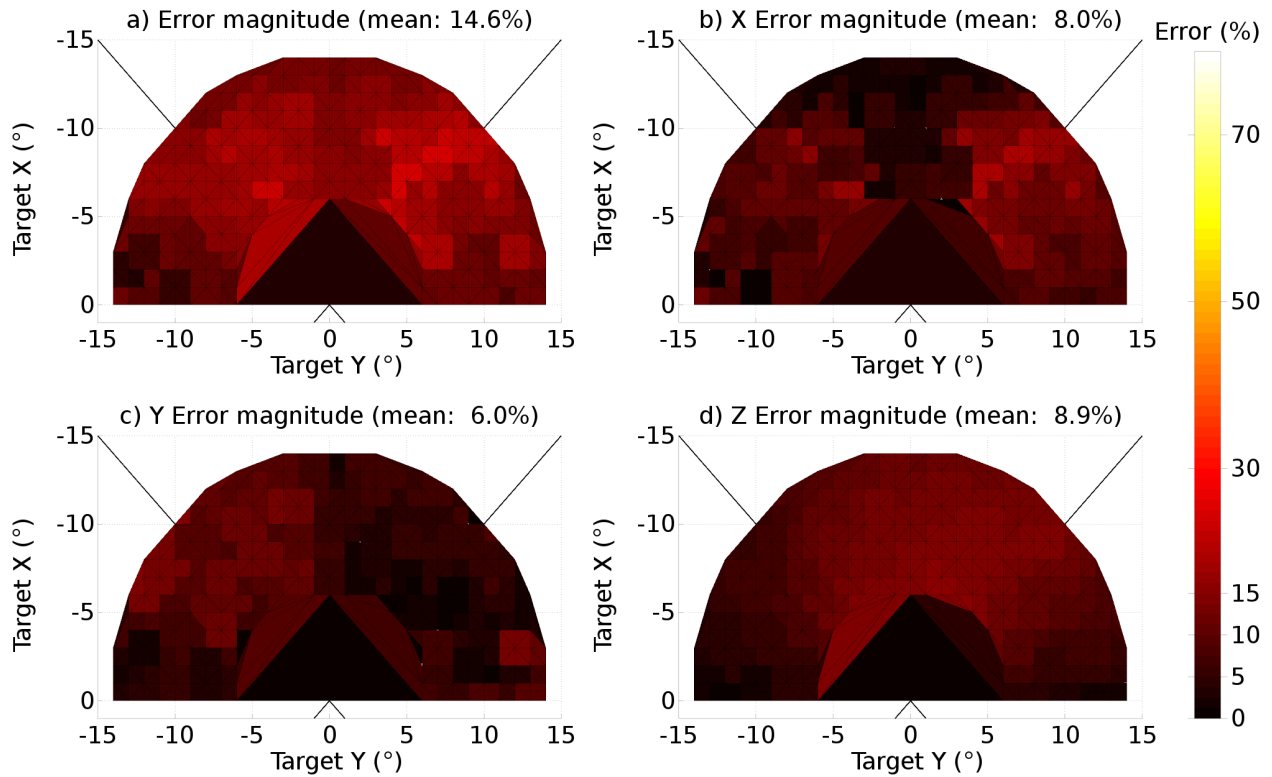


**Figure 11.** The end-point error surface for the model in which a widening projection field was added to the model of the superior colliculus. a) The ratio of the magnitudes of the total error vector and the target vector, expressed as a percentage. b) The ratio of the magnitude of the  $x$  component of the error vector to the magnitude of the target vector, expressed as a percentage. c) As (b) but for the  $y$  component. d) As (b), for  $z$  component. All colour maps are shown with the same scale. The target rotations,  $\theta_x^t$  and  $\theta_y^t$  are denoted ‘Target X’ and ‘Target Y’ in the figure. Note that the range of the colour scale is 0 to 20%, a much smaller range than the range in Fig 10.

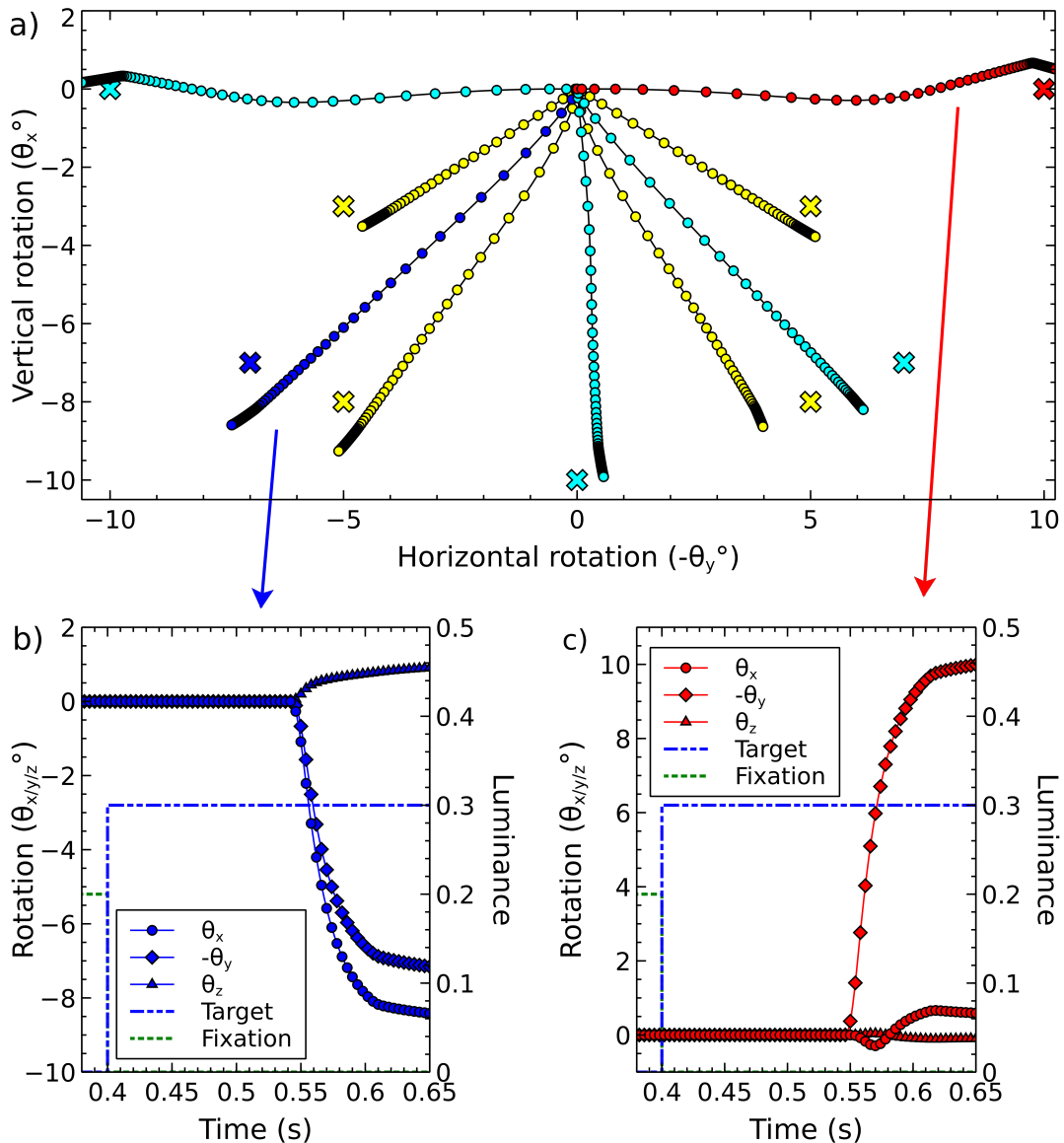


**Figure 12.** Representative single saccades. a) Trajectories from 9 saccades to a single target at 9 different locations. In each case, a fixation cross luminance of magnitude 0.2 was displayed at (0,0), the start position of the eye, until time 0.4 s. The target luminance, magnitude 0.3 was illuminated at time 0.4 s. Trajectory shape is dependent on the target position, and there is a variable amount of error in the end-points achieved by the model. Colour is used in this diagram as an aid to distinguishing different saccades and their targets; for a given saccade, the target location is given by the cross of the same colour closest to the end of the trajectory. b) The three rotational components of the ‘blue’ saccade, to target location (-7,-7). c) The three rotational components of the ‘red’ saccade, to target location (0,-10).

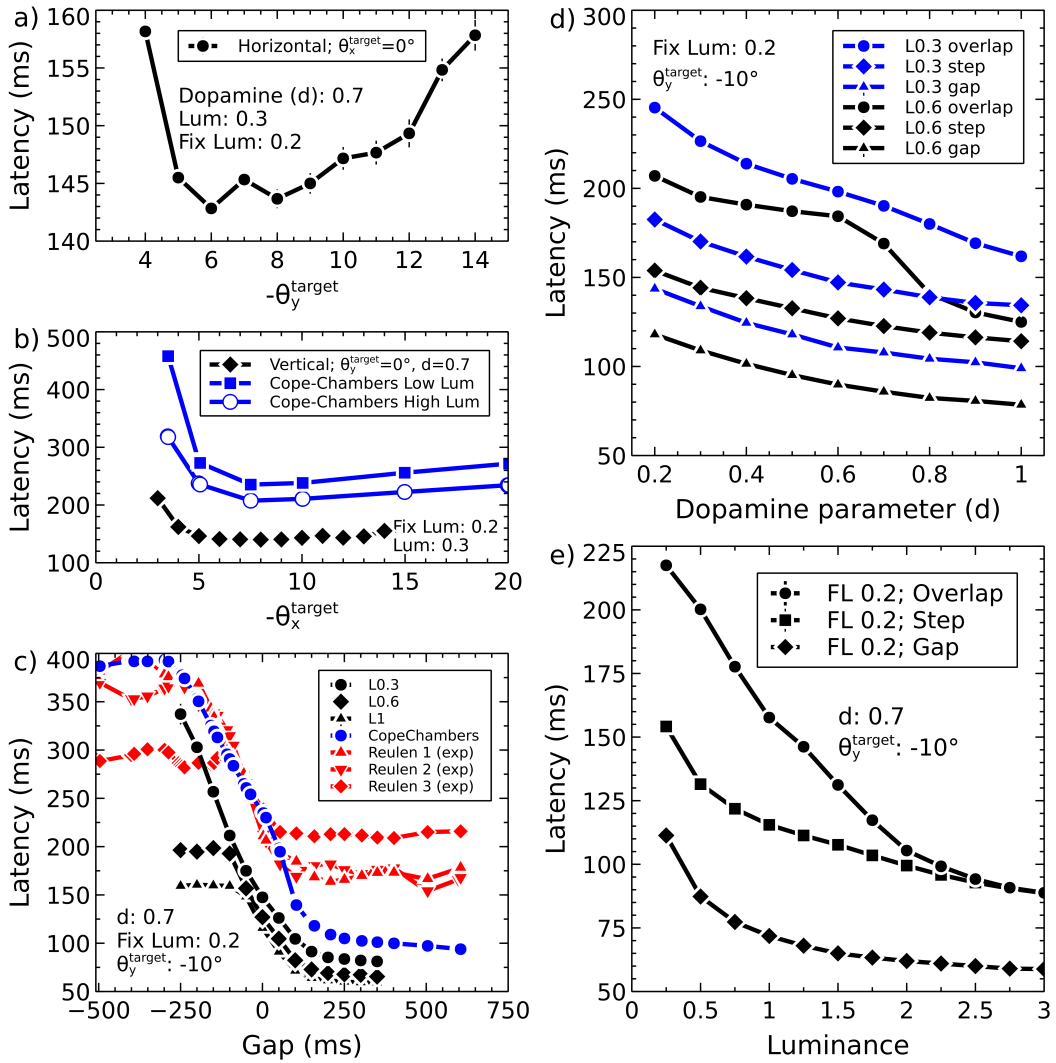


**Figure 13.** Exploring saccade latencies. a) Latency to first movement as a function of target eccentricity for horizontal targets. b) Latency vs. eccentricity for vertical targets. c) Latency vs. gap at three different luminance values. The data are shown alongside the Cope-Chambers model results from Fig. 5 of Cope et al. (2017) in blue, and the experimental results used in that model in red. The fixation luminance for the Cope-Chambers curve was 0.5, the target luminance 0.6 and the target eccentricity was  $8^\circ$ . The difference between the Cope-Chambers model data and the data from the current model results from the different mechanism by which activity in SC\_deep causes a movement, the differing target angle and the reduced fixation luminance used here. d) The effect of the dopamine parameter on saccade latencies in gap, step and overlap conditions, for two different target luminances. e) Saccade vs. luminance showing gradual transition between reflexive and express behaviour.

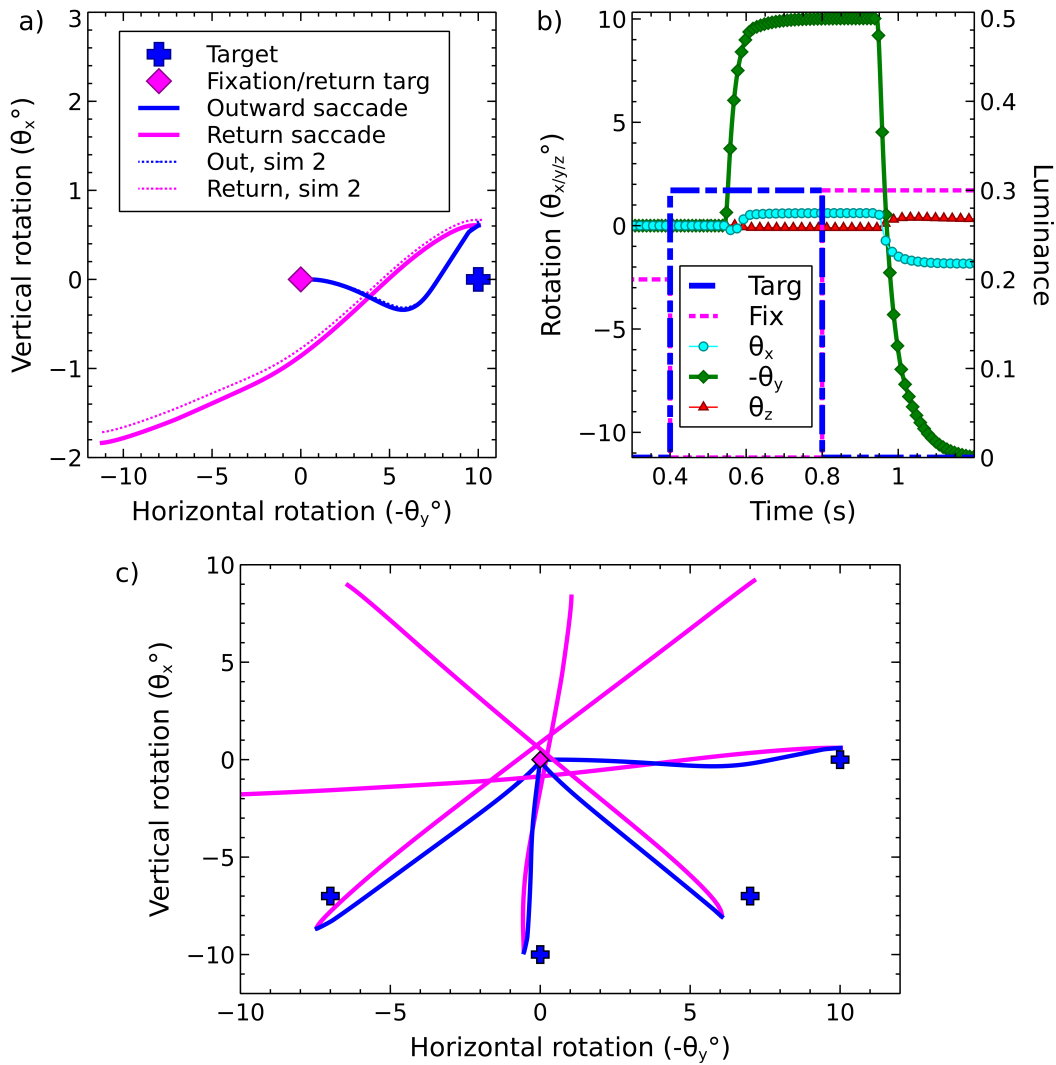


**Figure 14.** There and back - a saccade to a target, followed by return to the original fixation. a) Out and return saccade to a target at  $(0, -10^\circ)$  b) Rotational components of the saccade shown in (a). c) Outward and return trajectories for the saccade shown in (a) alongside saccades to three other targets.

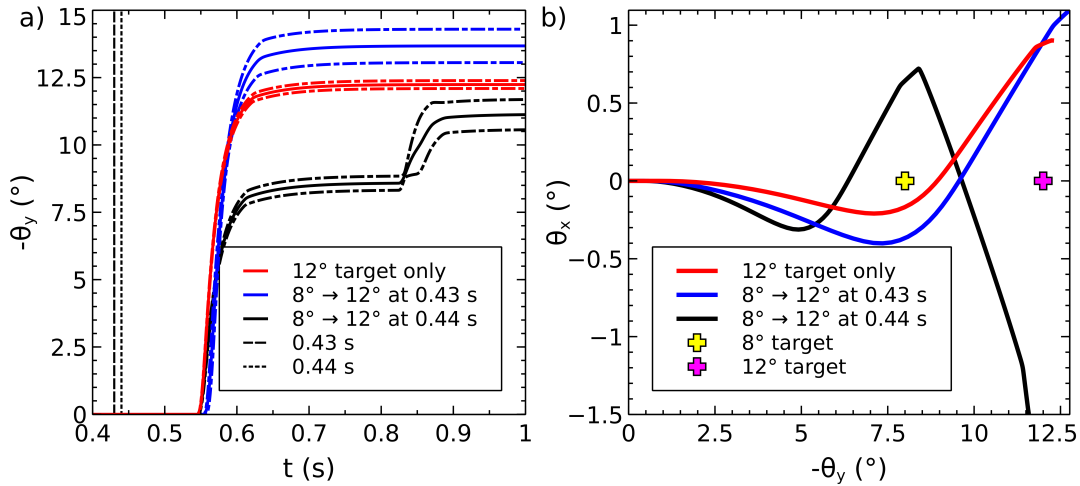


**Figure 15.** Double steps. The effect of illuminating a first target at  $8^\circ$  or  $12^\circ$ , followed by a second target at  $12^\circ$  or  $8^\circ$ . a) Horizontal rotation of the eye plotted vs. time for a saccade to the  $12^\circ$  target only (red), and to an  $8^\circ$  target at 0.4 s followed by a  $12^\circ$  target after 30 ms (blue) or 40 ms (black). The timings are indicated by vertical lines. When the second target is presented up to 30 ms after the initial target, the initial target has not had time to dominate the output saccade and a saccade to a location close to the second target is made. If the delay is 40 ms or more, the activity from the initial target has time to cause a built up of activity in SC\_deep and an initial saccade close to the first target is made, followed, after a longer than usual latency period, with a second saccade closer to the second target. In this graph, the mean of five separate simulations is plotted along with  $\pm 1$  standard deviation around the mean. b) The  $\theta_x/\theta_y$  trajectories corresponding to the data presented in (a).